

## Research papers

## Development and evaluation of a simple hydrologically based model for terrestrial evapotranspiration simulations

Gaofeng Zhu<sup>a,1,\*</sup>, Kun Zhang<sup>b,1,\*</sup>, Huiling Chen<sup>a</sup>, Yunquan Wang<sup>c</sup>, Yonghong Su<sup>d</sup>, Yang Zhang<sup>a</sup>, Jinzhu Ma<sup>a</sup>

<sup>a</sup> Key Laboratory of Western China's Environmental Systems (Ministry of Education), Lanzhou University, Lanzhou, China

<sup>b</sup> Institute of Tibetan Plateau Research, Chinese Academy of Sciences, Beijing, China

<sup>c</sup> School of Environmental Studies, China University of Geosciences, Wuhan, China

<sup>d</sup> Division of Hydrology Water-Land Research in Cold and Arid Regions, Northwest Institute of Eco-Environment and Resources, Chinese Academy of Sciences, Lanzhou, China

## ARTICLE INFO

This manuscript was handled by Emmanouil Anagnostou, Editor-in-Chief, with the assistance of Tao Yang, Associate Editor

## Keywords:

Evapotranspiration  
Transpiration  
Soil evaporation  
Soil water  
Hydrological model  
Priestly-Taylor

## ABSTRACT

Following the scheme of the groundwater-soil-plant-atmosphere continuum (GSPAC), a simple process-based model (SiTH; Simple Terrestrial Hydrosphere) was developed to estimate the dynamics of terrestrial evapotranspiration (ET) at the daily step. The input data include net radiation, air temperature, precipitation, leaf area index, vegetation type and soil data, most of which are readily available. Locally, the model performed well in simulating the dynamics of ET and soil moisture over selected FLUXNET sites. Globally, the daily 0.25° ET and groundwater table depth estimations in year 2005 were determined using available gridded datasets. The spatial pattern was reasonable and the range of values corresponded well with other global ET and groundwater table depth products. In future studies, we will produce a long-term daily 0.25° global ET and groundwater table depth products that spans from 1984 to present by using different input datasets.

## 1. Introduction

Evapotranspiration (ET), the sum of evaporation from bare soil, canopy interception stores, water body, sublimation from snow, and canopy transpiration through stomata, is an important land surface process in climatology and a nexus for terrestrial water, energy and carbon cycles (Fisher et al., 2008; Jung et al., 2010; Katul et al., 2012; Maxwell and Condon, 2016). About 60% of annual land precipitation is returned to the atmosphere through the ET process (Trenberth et al., 2007), and the associated latent heat of vaporization consumes more than 50% of the absorbed net solar radiation (Trenberth and Smith, 2009), which affects regional climate (Seneviratne et al., 2006). Therefore, accurate measurements and estimates of ET are crucial to a wide range of problems in hydrology (Xu and Singh, 1998; Zhu et al., 2013, 2014), geographical ecology (Fisher et al., 2011), climate change (Reynolds et al., 2000) and practical applications. Over the past decades, a large number of models, including simple or empirically-derived formulations, satellite-based algorithms, and land surface models (see e.g., Wang and Dickinson (2012) and Clark et al. (2015) for comprehensive reviews), have been developed to estimate ET at different

spatio-temporal scales, and are becoming more and more popular due to their advantages in addressing ecosystem processes over a spectrum of timescales (Shugart, 2000; Zhu et al., 2013).

Despite the aforementioned advancement, there are still some insufficiencies in parameterizing the basic hydrological processes in these models, which in turn limit our capability in accurately simulating the regional/global ET dynamics (Clark et al., 2015; Maxwell and Condon, 2016). First, there is increasing evidence that groundwater table dynamics have important impacts on root-zone soil moisture, surface runoff generation, land-atmosphere fluxes and regional climate (Clark et al., 2015), and different methods have been proposed to represent the groundwater table dynamics in land surface models (e.g., York et al., 2002; Liang et al., 2003; Maxwell and Miller, 2005; Yeh and Eltahir, 2005a,b; Niu et al., 2007; Miguez-Macho et al., 2008; Lo and Famiglietti, 2011; Miguez-Macho and Fan, 2012a,b; Fan et al., 2013; Maxwell and Condon, 2016). However, most of these methods are limited to regional-scale applications due to large computational and data requirements of their complex representations of groundwater dynamics (Maxwell and Miller, 2005; Lo and Famiglietti, 2011; Maxwell and Condon, 2016). Thus, there is a need to represent the

\* Corresponding authors.

E-mail addresses: zhugf@lzu.edu.cn (G. Zhu), zhangkun@itpcas.ac.cn (K. Zhang).

<sup>1</sup> Gaofeng Zhu and Kun Zhang contributed equally.

groundwater table dynamics in a parsimonious and computationally efficient way (Clark et al., 2015). Other methods often assume that the moisture flux exchange between unsaturated soil column and groundwater occurs at a fixed depth (York et al., 2002; Niu et al., 2007; Lo and Famiglietti, 2011; Fan et al., 2013), which may result in some significant biases in ET estimates (Koirala et al., 2014). Also, groundwater can act as the primary water source for ET when groundwater table is shallow (York et al., 2002). Thus, it is needed for models to properly quantify the proportion of ET from the different water sources (e.g., surface soil layer, deep soil layer and groundwater). Second, the plant root depth is not well parameterized by current ET models. Generally, most models assumed root depth of only 1.3–2.0 m in forests and 0.6–1.0 m in short vegetation (Choudhury et al., 1998; Gerten et al., 2004; Miralles et al., 2011). In fact, previous observations revealed widely varying rooting depths and broad associations with biome types (i.e. roots are shallow in boreal biomes and annual crops; deep roots are found in arid, semiarid, and season-arid climates) (Jackson et al., 1996; Canadell et al., 1996; Schenk and Jackson, 2002a,b). Thus, current models with unrealistically shallow root depths tend to underestimate the capability of the vegetation to resist drought and obtain a spuriously strong impact water stress on plant transpiration (Nepstad et al., 1994; Nobuhiro et al., 2007; Giambelluca et al., 2016; Giardina et al., 2018). Also, the root distribution has significant influences on the vertical profile of soil water content and groundwater table dynamics (Jackson et al., 1996). The improper representation of root distribution may result in significant biases in simulated soil moisture and groundwater table dynamics. Thus, to accurately estimate ET and its different components, it is needed to properly depict the basic hydrological processes and the interactions between hydrological processes and vegetation along the groundwater-soil-plant-atmosphere continuum (GSPAC) (Scanlon and Kustas, 2012).

This paper presents a new model, SiTH (Simple Terrestrial Hydrosphere) that was developed by coupling parsimonious and robust models of GSPAC, to estimate dynamics of terrestrial ET and its different components (soil evaporation, loss of intercepted water, and plant transpiration). The aims for the model were to (a) properly represent the groundwater table dynamics and its interaction with soil moisture, surface runoff and plant transpiration; (b) reduce the number of parameters and inputs as far as possible and facilitate its application to regional/global scale; (c) run on a daily frequency that could capture temporal variation in groundwater table dynamics and soil moisture, as well as their constraints on soil evaporation and plant transpiration; and (d) derive a global daily 0.25° ET (including its different components) and groundwater table depth dataset that can be used for studies of the global hydrological cycle. To examine the performances of our model, we validate model estimates with ground data from 85 FLUXNET sites representing a wide range of biomes and climate conditions; we also compared the distributions of global ET and groundwater table depth estimated by our model with other published studies.

## 2. Model description

The model, known as SiTH (Simple Terrestrial Hydrosphere), is designed to estimate terrestrial ET by incorporating the well-established models of each of the individual hydrological process over land (Fig. 1). The model is run on daily basis and contains six modules. In the first module, the canopy interception and evaporation loss of incident rainfall are calculated. The second module describes the snow accumulation and snowmelt dynamics. In the third module, the supply of water (i.e., throughfall, stemflow and snowmelt) is partitioned at land surface between surface runoff and infiltration. The fourth module is a two-layer soil water balance model that describes the vertical water movement in the unsaturated zone. The upper layer ( $z_1$ ) has a depth of 0–0.40 m, and the lower layer ( $z_2$ ) extends from  $z_1$  to the average root depths of different biomes (Jackson et al., 1996; Canadell et al., 1996; Schenk and Jackson, 2002a,b) (Table 1; Supplement 1). It is assumed

that soil evaporation is restricted to the upper layer, while plant transpiration can extract water from both layers. The fifth module is a simple groundwater model that describe the temporal variation of the groundwater table ( $z_{gw}$ ) in the unconfined aquifer. In this study, the groundwater table is defined as the depth at which the soil becomes saturated with water (Fig. 1). Finally, the potential evapotranspiration (PET), calculated using the Priestley and Taylor (PT) (1972) equation due to its minimal requirements for parameters and input variables, is downscaled to actual evapotranspiration based on ecophysiological constraints and water availability. The framework of the model, separated into input, main module and output domains, are given in Fig. 2. A detail description of entire hydrological flux computations is given in the following sections.

### 2.1. Rainfall interception loss

In SiTH, precipitation ( $P_r$ , mm day $^{-1}$ ) is divided into rainfall ( $R_a^{\text{fall}}$ , mm day $^{-1}$ ) and snowfall ( $S_n^{\text{fall}}$ ; mm day $^{-1}$ ) depending on whether daily mean air temperature is above or below 0 °C. All precipitation on days with negative daily mean temperature adds to snowpack; snowfall interception is omitted due to the lack of proper candidate models (Miralles et al., 2010). Rainfalls intercepted by the canopy are evaporated at the potential rate. The capacity of canopy to store water ( $S_c$ , mm day $^{-1}$ ) is defined as a function of biome, incoming rainfall ( $R_a^{\text{fall}}$ , mm day $^{-1}$ ), and leaf area index (LAI) (Kergoat, 1998):

$$S_c = \beta \times R_a^{\text{fall}} \times \text{LAI}$$

where  $\beta$  us a dimensionless biome-dependent coefficient for the rainfall regime (Table 1). The fraction of day-time consumed by wet canopy evaporation,  $f_{\text{wet}}$ , is calculated as (Kergoat, 1998):

$$f_{\text{wet}} = \min\{\chi \frac{S_c}{T_p}, 1\}$$

where  $T_p$  (mm day $^{-1}$ ) is the potential transpiration rate of canopy (see below);  $\chi$  is fractional interception occurring during day-time, which is primarily governed by diurnal variation of precipitation. For 50%–90% of rainfall occurring during day-time, the range of  $\chi$  could be 0.5–0.9 due to diurnal variation of precipitation (Oki and Musiake, 1994). Here, the value of  $\chi$  is set to be 0.7. Daily interception loss ( $E_i$ ; mm day $^{-1}$ ) is then given by:

$$E_i = f_{\text{wet}} \times T_p$$

The remaining day-time canopy-available energy ( $1 - f_{\text{wet}}$ ) is used for plant transpiration (see below).

### 2.2. Snowpack water balance

For high latitudes and mountainous regions, the water balance is largely controlled by snow processes. In SiTH, the snow water balance equation is simply expressed as:

$$\frac{dS_w}{dt} = S_n^{\text{fall}} - S_m - E_s'$$

where  $S_w$  is snowpack water content (mm);  $S_n^{\text{fall}}$  is daily snow fall (mm day $^{-1}$ );  $S_m$  is daily snowmelt (mm day $^{-1}$ );  $E_s'$  is net snow evaporation (mm day $^{-1}$ ); and  $t$  is time index with an interval length of 1 day. Snowmelt is calculated using the degree-day method (Choudhury et al., 1998):

$$S_m = (1.5 + 0.007S_n^{\text{fall}}) \times T_a$$

where  $T_a$  is air temperature above 0 °C. Research on snow evaporation and condensation are rather limited (Gray and Prowse, 1993). Following Choudhury and DiGirolamo (1998), a constant  $E_s'$  of 0.15 mm day $^{-1}$  is used for the duration of snow cover.

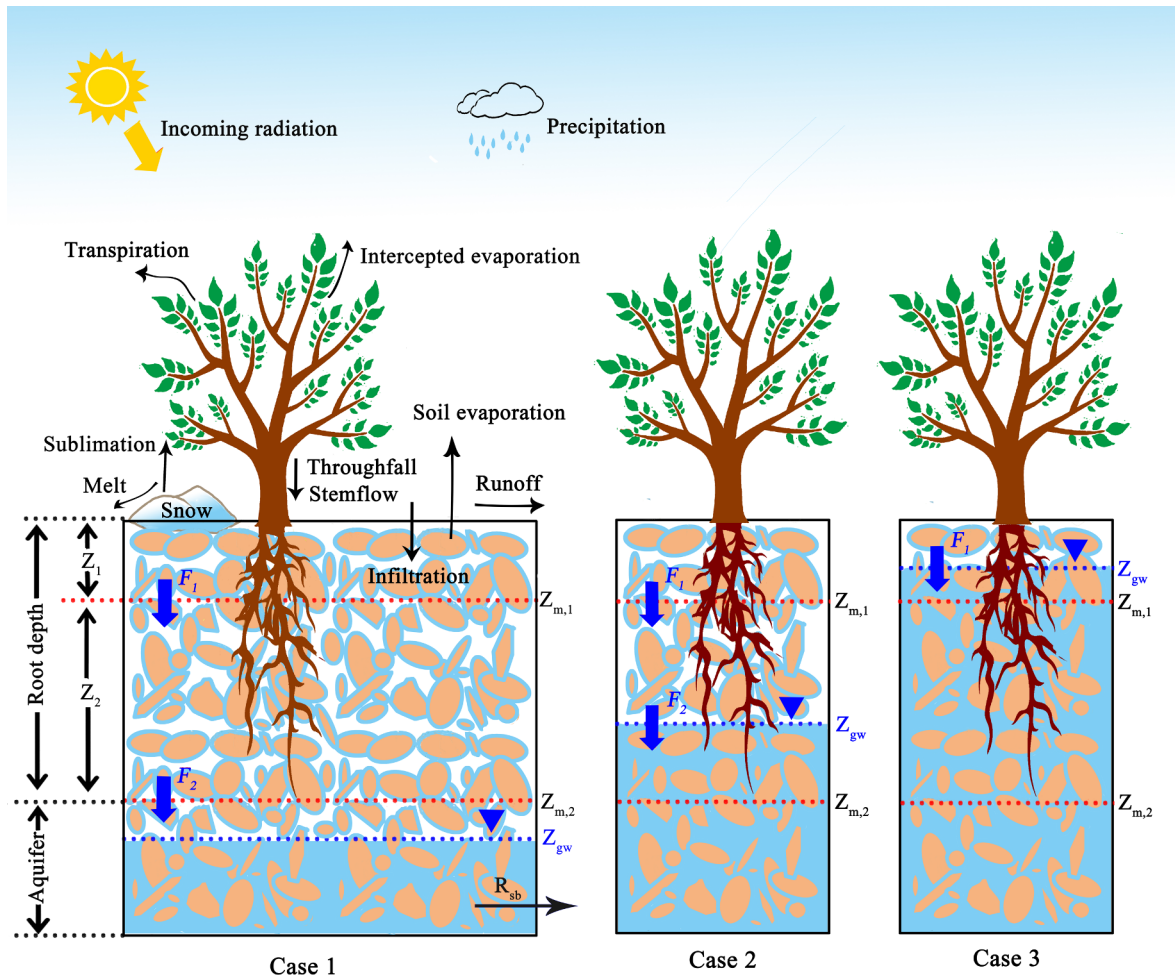


**Fig. 1.** Schematic representation of the hydrological process computed by the SiTH model. Case 1 represents that groundwater table is below the root zone; and Case 2 and Case 3 represent that groundwater table is within the second and first soil layer, respectively. The arrows indicate water fluxes.

**Table 1**  
Hydrologically relevant biome parameter values.

PFTs	$\beta$	$D_{50}$ (cm)	$c$	$Z_r$ (m)
tropical evergreen broadleaf tree	0.02	15	-1.63	7.3
tropical raingreen broadleaf tree	0.02	16	-1.65	3.7
temperate evergreen needleleaf tree	0.06	21	-1.84	3.9
temperate evergreen broadleaf tree	0.02	23	-1.77	7.0
temperate deciduous broadleaf tree	0.02	23	-1.77	2.9
boreal evergreen needleleaf tree	0.06	12	-1.87	2.0
boreal deciduous needleleaf tree	0.06	12	-1.87	2.0
boreal deciduous broadleaf tree	0.06	12	-1.87	2.0
grass	0.01	13	-1.92	2.6
humid tropical savannas	0.01	14	-1.54	8.0
dry tropical savannas	0.01	28	-1.80	15
temperate savanna	0.01	23	-1.63	8.0
mediterranean shrub	0.01	19	-1.34	5.2
desert shrub	0.01	28	-1.91	9.5
tundra	0.01	9	-2.51	0.5
crop	0.01	18	-2.01	2.1

$\beta$ : the coefficient for calculation of interceptions;  $D_{50}$  and  $c$ : the shape parameters of logistic dose-response root distribution model;  $Z_r$ : root depth (m).

### 2.3. Surface runoff

Surface runoff,  $R_s$  (mm day $^{-1}$ ), is estimated using the Soil Conservation Service (SCS) curve number technique (SCS, 1985, 1986):

$$R_s = \begin{cases} \frac{(P_{\text{net}} - 0.2 \times V_{\max})^2}{P_{\text{net}} + 0.8 \times V_{\max}} & P_{\text{net}} > 0.2V_{\max} \\ 0 & P_{\text{net}} \leq 0.2V_{\max} \end{cases} \quad (6)$$

where  $P_{\text{net}}$  (mm day $^{-1}$ ) is the daily flux of water incident on soil surface (i.e.,  $P_{\text{net}} = P_r - E_t + S_m$ ); and  $V_{\max}$  (mm) is the overall soil water retention capacity, which can be estimated as (Choudhury and DiGirolamo, 1998):

$$V_{\max} = \sum_{i=1}^2 (\theta_{s,i} - \theta_{a,i}) \times d_i \quad (7)$$

where  $\theta_{s,i}$  ( $\text{m}^3 \text{ m}^{-3}$ ) and  $\theta_{a,i}$  ( $\text{m}^3 \text{ m}^{-3}$ ) is the saturated and antecedent (previous day) soil water content for the  $i$ th soil layer ( $i = 1$  and 2), respectively;  $d_i$  is the thickness of the unsaturated soil in the  $i$ th layer (mm). In SiTH, the depth of root zone remains constant for each biome, but the thickness of unsaturated soil in each layer is variable with time as the groundwater table depth dynamically changes (Fig. 1). Thus, the thickness of the unsaturated soil in the  $i$ th layer ( $d_i$ ,  $i = 1, 2$ ) is calculated as:

$$d_i = \begin{cases} 0 & z_{gw} \leq z_{m,i-1} \\ z_{gw} - z_{m,i-1} & z_{m,i-1} < z_{gw} \leq z_{m,i} \\ z_i & z_{gw} > z_{m,i} \end{cases} \quad (8)$$

where  $z_i$  is the depth of the  $i$ th soil layer (mm);  $z_{m,i}$  is the bottom depth of the  $i$ th layer (note that for the first layer ( $i = 1$ ), the value of  $z_{m,i-1}$  is equal to zero); and  $z_{gw}$  is the groundwater table depth from the surface (mm) (Fig. 1). As an example, when the groundwater table reaches the

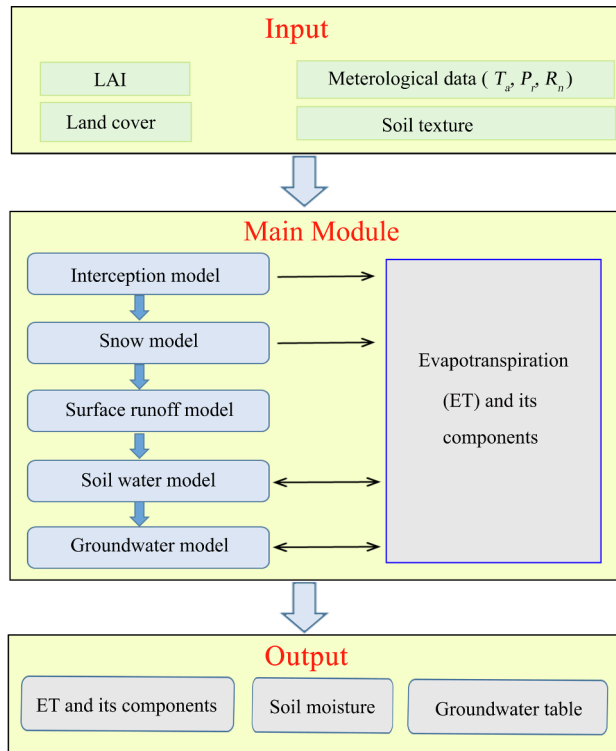


**Fig. 2.** Inputs and outputs of the model, and major modules affecting ET. Soil moisture changes are determined by estimating soil water balance at daily time step. Both soil moisture and groundwater table depth affect ET because the groundwater table can seasonally rise to within the root zone. ET in turn affects both soil moisture and groundwater table depth.

surface ( $z_{gw} = 0$ ; meaning that the whole soil profile is saturated), both  $d_1$  and  $d_2$  will be equal to zero and the entire volume of net precipitation ( $P_{net}$ ) becomes surface runoff (Eq. (6)). The amount of water infiltrating into the soil ( $I_n$ ; mm day $^{-1}$ ) is expressed as the minimum of two factors as follows:

$$I_n = \min\{K_{s,1}, P_{net} - R_s\} \quad (9)$$

where  $K_{s,1}$  is the saturated hydraulic conductivity of the first soil layer (mm day $^{-1}$ ) (Table 2).

**Table 2**  
Representative values for hydraulic parameters in each soil textural class.

Class	$K_s$ (m day $^{-1}$ )	$\psi_s$ (m)	$\theta_s$ (m $^3$ m $^{-3}$ )	$b$ (-)	$\theta_{fc}$ (m $^3$ m $^{-3}$ )	$\theta_c$ (m $^3$ m $^{-3}$ )	$\theta_w$ (m $^3$ m $^{-3}$ )
Sand	1.3841	-0.0232	0.373	3.39	0.151	0.109	0.035
Loamy sand	0.8229	-0.0175	0.386	3.86	0.189	0.142	0.052
Sandy loam	0.5353	-0.0316	0.416	4.50	0.265	0.208	0.087
Loam	0.4086	-0.0655	0.435	5.77	0.331	0.274	0.139
Silty loam	0.4427	-0.0471	0.468	4.98	0.399	0.320	0.146
Sandy clay loam	0.4991	-0.0310	0.416	7.20	0.314	0.270	0.157
Clay loam	0.3552	-0.0599	0.449	8.32	0.387	0.339	0.212
Silty clay loam	0.3848	-0.0414	0.476	8.32	0.444	0.389	0.243
Sandy clay	0.6157	-0.0269	0.423	9.59	0.349	0.312	0.207
Silty clay	0.2967	-0.0453	0.481	10.4	0.460	0.414	0.284
Clay	0.2580	-0.0531	0.461	12.1	0.427	0.90	0.282

$K_s$ ,  $\psi_s$ , and  $\theta_s$ : the hydraulic conductivity, water potential and water content at saturation condition, respectively;  $b$ : an empirical parameter;  $\theta_{fc}$ ,  $\theta_c$ , and  $\theta_w$ : soil moisture at field capacity, critical value, and wilting point, respectively.

## 2.4. Soil water balance

The vertical movement of soil moisture in unsaturated layers is simulated using a two-layer model. The infiltration water ( $I_n$ ; mm day $^{-1}$ ) was first stored in the top unsaturated layer, which subsequently drained to field capacity into the next soil layer (Allen et al., 1998; Miralles et al. 2011); and the same procedure was used to calculate the vertical flow from the remaining layers until it finally recharges to the underlying groundwater (Fig. 1). Here, this empirical drainage algorithm is preferred over well known alternatives such as the Richards equation (Richards, 1931), due to its simplicity and relatively high computational efficiency for the global-scale simulations. At every daily time step, the soil water content in each unsaturated layer is modelled as:

$$\begin{cases} d_1 \times \frac{d\theta_1(t)}{dt} = I_n(t) - E_s(t) - T_{s,1}(t) - F_1(t) \\ d_2 \times \frac{d\theta_2(t)}{dt} = F_1(t) - T_{s,2}(t) - F_2(t) \end{cases} \quad (10)$$

where  $\theta_i$  (m $^3$  m $^{-3}$ ) is water content of unsaturated soil in the  $i$ th layer ( $i = 1$  and  $2$ );  $d_i$  (mm) is the thickness of the unsaturated soil in the  $i$ th layer;  $I_n$  (mm day $^{-1}$ ) is the entire volume of infiltration water;  $E_s$  (mm day $^{-1}$ ) is daily actual soil evaporation (see below);  $T_{s,i}$  (mm day $^{-1}$ ) is daily plant transpiration from the unsaturated soil in the  $i$ th layer (see below); and  $F_i$  (mm day $^{-1}$ ) denotes the drainage of water out of the  $i$ th layer, which is estimated as:

$$F_i(t) = \max\{0, d_i \times [\theta_i(t) - \theta_{fc,i}]\} \quad (11)$$

where  $\theta_{fc,i}$  (m $^3$  m $^{-3}$ ) is the field capacity of the  $i$ th soil layer. In SiTH, the groundwater table depth determines the number of unsaturated layers in root zone and the thickness of the unsaturated soil in each layer ( $d_i$ ,  $i = 1, 2$ ), as well as the position of the interface between the soil and the groundwater (Fig. 1). This is more realistic than assumption of a fixed depth for flux exchange between the unsaturated soil column and the aquifer that adopted by most land surface models (Clark et al., 2015). In addition, the water drainage out of the unsaturated zone to groundwater may be available for plant transpiration in SiTH if the groundwater table extents to the root zone and therefore affects the modelled ET.

## 2.5. Groundwater mass balance

The temporal variation of water stored in the saturated zone,  $W_a$  (mm), is expressed as:

$$\frac{dW_a}{dt} = F_i - T_{r,g} - R_{sb} \quad (12)$$

where  $i$  is the index of soil layer that directly drains water to the underlying groundwater (Fig. 1);  $F_i$  (mm day $^{-1}$ ) is the flux draining from the  $i$ th soil layer to recharge the groundwater (Eq. (11));  $T_{r,g}$  is plant transpiration from the groundwater when the water table resides in the root zone (see below); and  $R_{sb}$  (mm day $^{-1}$ ) is the groundwater discharge, which is parameterized as (Niu et al., 2007):

$$R_{sb} = R_{sb,max} e^{-f \times z_{gw}} \quad (13)$$

where  $R_{sb,max}$  (mm day $^{-1}$ ) is the maximum groundwater discharge when the groundwater table depth is zero; and  $f$  (mm $^{-1}$ ) is the e-fold depth. Following Niu et al. (2007), the values of  $R_{sb,max}$  and  $f$  are set to be 39 mm day $^{-1}$  and  $1.25 \times 10^{-3}$  mm $^{-1}$ , respectively. Then, the change in water tabel depth ( $z_{gw}$ ; mm) is calculated from:

$$\frac{dz_{gw}}{dt} = \begin{cases} \frac{1}{\theta_{s,i} - \theta_i} \times \frac{dW_a}{dt} & z_{m,i-1} < z_{gw} \leq z_{m,i} \\ \frac{1}{S_y} \times \frac{dW_a}{dt} & z_{gw} > z_{m,2} \end{cases} \quad (14)$$

where  $i$  is the index of soil layer where the groundwater table resides;  $\theta_{s,i}$  and  $\theta_i$  is the saturated and current soil water content of the  $i$ th soil

layer, respectively; and  $S_y$  is the specific yield of the unconfined aquifer, which is set to be 0.2 in the global simulations due to the dearth of specific yield data for global aquifers (Niu et al., 2007).

## 2.6. Potential evapotranspiration

The Priestley-Taylor (PT) (Priestley and Taylor, 1972) equation, which is a function of available energy and a dimensionless coefficient ( $\alpha$ ), works well as a potential evapotranspiration (PET) model for each component flux (Gerten et al., 2004; Fisher et al., 2008; Miralles et al., 2011). Assuming a homogeneous canopy, the potential canopy transpiration ( $T_p$ ; mm day $^{-1}$ ) and soil evaporation ( $E_p$ ; mm day $^{-1}$ ) can be calculated as (Fisher et al., 2008):

$$T_p = \alpha \frac{\Delta}{\Delta + \gamma} R_{nc} \quad (15)$$

$$E_p = \alpha \frac{\Delta}{\Delta + \gamma} \frac{(R_{ns} - G)}{\lambda} \quad (16)$$

where  $\lambda$  is the latent heat of vaporization (MJ kg $^{-1}$ );  $\Delta$  is the slope of the saturation vapor pressure versus temperature curve (kPa K $^{-1}$ );  $\gamma$  is the psychrometric constant (kPa K $^{-1}$ );  $G$  is the soil heat flux (MJ day $^{-1}$ );  $R_{nc}$  (MJ day $^{-1}$ ) is the net radiation to the canopy and is given by  $R_{nc} = R_n - R_{ns}$ , where  $R_n$  (MJ day $^{-1}$ ) is the net radiation and  $R_{ns}$  (MJ day $^{-1}$ ) is the net radiation to the soil.  $R_{ns}$  is calculated according to the Beer's law:

$$R_{ns} = R_n \exp(-k_{R_n} \times LAI) \quad (17)$$

where  $k_{R_n}$  is the extinction coefficient, which is set to be 0.6 (Impens and Lemur, 1969). In SiTH, a constant of value of  $\alpha = 1.26$  used so that the PT equation as a PET equation remains intact as originally designed and confirmed (Fisher et al., 2008). When soil heat flux measurements are not available, it is calculated as (Choudhury et al., 1987):

$$G = 0.4 \times R_n \times \exp(-0.5 \times LAI) \quad (18)$$

The maximum transpiration rate of each soil layer ( $T_{p,i}$ ;  $i = 1$  and 2) depends on the root fraction and soil moisture condition within the layer, which is calculated as (Tiktak and Bouten, 1992):

$$T_{p,i} = \frac{r_i \times (\bar{\theta}_i / \theta_{s,i})^b}{\sum_{i=1}^2 [r_i \times (\bar{\theta}_i / \theta_{s,i})^b]} \times T_p \quad (19)$$

where  $b$  (dimensionless) is a soil parameter, which depends on soil physical properties (Table 2);  $\theta_{s,i}$  is the saturated water content in the  $i$ th soil layer;  $r_i$  (dimensionless) represents the vertical root density at the  $i$ th soil layer; and  $\bar{\theta}_i$  is the layer mean water content, which is calculated as:

$$\bar{\theta}_i = \begin{cases} \theta_{s,i} & z_{gw} \leq z_{m,i-1} \\ \frac{\theta_i(z_{gw} - z_{m,i-1}) + \theta_{s,i}(z_{m,i} - z_{gw})}{z_i} & z_{m,i-1} < z_{gw} \leq z_{m,i} \\ \theta_i & z_{gw} > z_{m,i} \end{cases} \quad (20)$$

where  $\theta_i$  ( $i = 1, 2$ ) is the unsaturated soil water content in the  $i$ th soil layer;  $z_{m,i-1}$  and  $z_{m,i}$  is the bottom depth of the  $(i-1)$ th and  $i$ th layer, respectively;  $z_i$  is the depth of the  $i$ th soil layer; and  $z_{gw}$  is the groundwater table depth (Fig. 1). In SiTH, the vertical root density,  $r_i$ , is described by the linear dose response (LDR) model (Schenk and Jackson, 2002a):

$$r_i = \frac{1}{1 + (z_{m,i}/D_{50})^c} - \frac{1}{1 + (z_{m,i-1}/D_{50})^c} \quad (21)$$

where  $D_{50}$  is the depth above which 50% of the root mass is located;  $c$  is a shape parameter; and  $z_{m,i}$  is the bottom depth of the  $i$ th layer (Fig. 1). The values of  $D_{50}$  and  $c$  for different plant function types (PFTs) are presented in Table 1.

In SiTH, plant can extract water from either the soil or groundwater, or both of a specific layer depending on the position of groundwater

table (Fig. 1). To conserve the mass balance, the total potential transpiration partitioned in the  $i$ th layer,  $T_{p,i}$ , is further separated into the soil and groundwater components based on the thickness-weighted water content. The potential transpiration from soil water of the  $i$ th layer,  $T_{p,s,i}$  (mm day $^{-1}$ ) ( $i = 1, 2$ ), is calculated as:

$$T_{p,s,i} = \begin{cases} 0 & z_{gw} \leq z_{m,i-1} \\ \frac{(z_{gw} - z_{m,i-1})\bar{\theta}_i}{(z_{gw} - z_{m,i-1})\bar{\theta}_i + (z_{m,i} - z_{gw})\bar{\theta}_{s,i}} T_{p,i} & z_{m,i-1} < z_{gw} \leq z_{m,i} \\ T_{p,i} & z_{gw} > z_{m,i} \end{cases} \quad (22)$$

The potential transpiration from groundwater in the  $i$ th layer,  $T_{p,g,i}$  (mm day $^{-1}$ ) ( $i = 1, 2$ ), is calculated as:

$$T_{p,g,i} = \begin{cases} T_{p,i} & z_{gw} \leq z_{m,i-1} \\ \frac{(z_{m,i} - z_{gw})\bar{\theta}_{s,i}}{(z_{gw} - z_{m,i-1})\bar{\theta}_i + (z_{m,i} - z_{gw})\bar{\theta}_{s,i}} T_{p,i} & z_{m,i-1} < z_{gw} \leq z_{m,i} \\ 0 & z_{gw} > z_{m,i} \end{cases} \quad (23)$$

For example, when groundwater table is below the root zone ( $z_{gw} > z_{m,2}$ ), the values of  $T_{p,g,i} = 0$  and  $T_{p,s,i} = T_{p,i}$  ( $i = 1, 2$ ) and plant transpiration only consumes soil water in root zone and has no effects on the modelled groundwater table. When groundwater is within root zone, plant transpiration will reduce both the water content of unsaturated soil and the water table depth.

## 2.7. Actual evapotranspiration

As a result of suboptimal environmental conditions, the actual fluxes of plant transpiration and soil evaporation are generally lower than their potential values. In SiTH, three reduction factors were used to downscale the potential transpiration ( $T_p$ ) to the actual value: (i) soil moisture stress ( $f_{SM}$ ); (ii) plant temperature constraint ( $f_T$ ); and (iii) the time lost to transpiration due to the wet canopy fraction ( $f_{wet}$ ), which is given in Eq. (2). Thus, the actual transpiration from the unsaturated soil at the  $i$ th layer ( $T_{s,i}$ ) was obtained as:

$$T_{s,i} = (1 - f_{wet}) \times f_{SM,i} \times f_T \times T_{p,s,i}$$

where  $f_{SM,i}$  and  $f_T$  are calculated as (June et al., 2004; Fisher et al., 2008; Miralles et al., 2011):

$$f_{SM,i} = \begin{cases} 0 & \theta_i \leq \theta_{wp,i} \\ 1 - \left( \frac{\theta_{c,i} - \theta_i}{\theta_{c,i} - \theta_{wp,i}} \right)^2 & \theta_{wp,i} < \theta_i < \theta_{c,i} \\ 1 & \theta_i \geq \theta_{c,i} \end{cases} \quad (25)$$

$$f_T = \exp \left[ - \left( \frac{T_a - T_{opt}}{T_{opt}} \right)^2 \right] \quad (26)$$

where  $\theta_i$  (m $^3$  m $^{-3}$ ) is the soil moisture of  $i$ th layer;  $\theta_{c,i}$  (m $^3$  m $^{-3}$ ) is the soil moisture below which plants start to endure water stress for soil layer  $i$  (Laio et al., 2001);  $\theta_{wp,i}$  (m $^3$  m $^{-3}$ ) is soil moisture at permanent wilting point;  $T_a$  (°C) is the daily mean air temperature; and  $T_{opt}$  (°C) is the optimum temperature for canopy transpiration, which is defined as the daily air temperature when leaf area, net radiation and temperature are high (Potter et al., 1993). For transpiration from groundwater, only the constraints of temperature ( $f_T$ ) and wet canopy fraction ( $f_{wet}$ ) are considered. The total of volume transpiration from groundwater that caused groundwater table to decline is then calculated as:

$$T_{r,g} = (1 - f_{wet}) \times f_T \times \sum_{i=1}^n T_{p,g,i} \quad (27)$$

where  $n$  is the number of layers that contain both plant root and groundwater (i.e.,  $n = 1$ , if  $z_{gw} > z_{m,1}$ ; and  $n = 0$ , if  $z_{gw} > z_{m,2}$ ).

Soil evaporation declines as the soil gets dry, and is assumed to be affected only by the unsaturated soil water content in the upper layer ( $i = 1$ ). Thus, the actual soil evaporation ( $E_s$ ) is calculated as:

$$E_s = f_{SM} \times E_p \quad (28)$$

where  $f_{SM}$  is given as (Miralles et al., 2011):

$$f_{SM} = \begin{cases} 0 & \theta_1 \leq \theta_{wp,1} \\ 1 - \left( \frac{\theta_{c,1} - \theta_1}{\theta_{c,1} - \theta_{wp,1}} \right)^{\frac{1}{2}} & \theta_{wp,1} < \theta_1 < \theta_{c,1} \\ 1 & \theta_1 \geq \theta_{c,1} \end{cases} \quad (29)$$

where  $\theta_1$  is the unsaturated soil moisture in the upper layer ( $m^3 m^{-3}$ ). The values of  $\theta_{wp}$  and  $\theta_c$  for each layer were calculated using the soil water retention function with the soil water potentials of  $\psi_{wp} = -150$  m and  $\psi_c = -3$  m, respectively, and data for 11 different soil types are given in Table 2 based on the works of Clapp and Hornberger (1978) and Cosby et al. (1984). A detail description about soil water stress functions for different soil types was given in Supplement 1.

### 3. Data and methods

#### 3.1. Eddy covariance flux data for model validation

The recently released FLUXNET2015 dataset (<http://fluxnet.fluxdata.org/data/fluxnet2015-dataset/>; Pastorello et al., 2017) provides an invaluable wealth of flux data, complemented by meteorological variables and soil moisture. For validation purpose, the sites in the FLUXNET2015 dataset were selected in such a way that they cover a wide range of vegetation types and climates. In addition to this, the data needed to span at least one year after a station by station quality check, which is defined as following: (i) when the measured energy imbalance (net radiation minus latent, sensible, and ground heat flux) exceeds  $250 W m^{-2}$ , the half-hourly (hourly) flux data were treated as missing; (ii) when the data gaps were less than 6 h in a day, the missing data was interpolated using linear regression method; (iii) any day that did not have necessary measurements to complete a diurnal cycle was not used in the analysis of model evaluations; and (iv) rainy intervals were masked from the in situ flux datasets as the eddy covariance measurements are less reliable during precipitation events. This yielded a total of 84 reliable eddy covariance sites, which are located across several continents and cover a large variety of ecosystems (Table S1 in Supplement 2). The energy balance closure across the selected sites ranges from 70% to 99% with a mean of 80.2%, and the intercept values range  $-22.4$  to  $26.1 W m^{-2}$  with a mean of  $-1.24 \pm 10.5 W m^{-2}$  (Table S2 in Supplement 2). Therefore, the processed flux data was qualified and suitable for the purposes of model validations. To account for the biased low in situ ET measurements due to the energy imbalance at the selected sites (1%–30%), the directly measured ET data were corrected by using the residual energy balance method (Twine et al., 2000). Among the selected sites in FLUXNET dataset, 38 sites also provide in situ soil moisture measurements approximately over the top 30 cm of the soil (Novick et al., 2016). The sites reporting both soil moisture and ET measurements were labeled as focus sites (Table S1 in Supplement 1), and used to test model accuracy in simultaneously simulating ET and soil water content. Due to limited observational soil moisture data for deep soil layers, we only compared the modeled soil moisture of the first layer ( $\theta_1$ ; 0–20 cm) with in situ measurements at the top-soil (SWC1 in the FLUXNET2015 dataset).

For validation purposes, in situ measured meteorological variables from the flux towers, which include surface net radiation ( $R_n$ ;  $W m^{-2}$ ), soil heat flux ( $G$ ,  $W m^{-2}$ ), air temperature ( $T_a$ ,  $^{\circ}C$ ), and precipitation ( $P_r$ ;  $mm day^{-1}$ ), were used to drive the model to simulate ET and soil water contents. The leaf area index (LAI) required by the model were extracted from Moderate Resolution Imaging Spectroradiometer (MODIS) product (MOD15A2H) (<https://lpdaac.usgs.gov/>; Myneni et al., 2015) at 500 m spatial and 8 day temporal resolution. An average of nine surrounding pixels around the FLUXNET2015 sites was used to calculate the required LAI values. Data were cleaned by eliminating

contamination associated with clouds, shadows and snow/ice, and were interpolated to daily values using the linear interpolation approach (Zhang et al., 2010).

The performance of SiTH model in simulating ET and soil water content was evaluated by using the coefficient of determination ( $R^2$ ), slope ( $b_0$ ) and intercept ( $b_1$ ) of the regression line ( $y = b_0 \times x + b_1$ ) between the measured ( $x$ ) and estimated ( $y$ ) values. Model-data mismatch was also quantified using root-mean-squared error (RMSE), mean bias error (MBE), and the Nash-Sutcliffe efficiency coefficient (NSE). These were calculated as:

$$RMSE = \sqrt{\frac{1}{n} \sum_{t=1}^n [O(t) - M(t)]^2} \quad (30)$$

$$MBE = \frac{\sum_{t=1}^n [O(t) - M(t)]}{n} \quad (31)$$

$$NSE = 1 - \frac{\sum_{t=1}^n [O(t) - M(t)]^2}{\sum_{t=1}^n [O(t) - \bar{O}]^2} \quad (32)$$

where  $n$  is the total number of observations;  $O(t)$  is the observed values at time  $t$ ,  $\bar{O}$  is the mean of the observed data, and  $M(t)$  is the model predictions at time  $t$ . The coefficient of determination ( $R^2$ ) describes the degree of co-linearity between observed and simulated values and ranges between 0 and 1, with higher values indicating less error variance. Generally, an  $R^2 > 0.5$  is considered as acceptable performance (Moriasi et al., 2007). For MBE, a positive MBE indicates an overall overestimation while a negative MBE indicates an overall underestimation. The closer the MBE to zero, the better is the model's performance. The NSE value can range between  $-\infty$  and 1.0, with a NSE = 1 being the optimal value (Moriasi et al., 2007; Zhu et al., 2016).

#### 3.2. Gridded datasets for global implementation and evaluation

For global estimates of ET, the forcing datasets used to run SiTH model included precipitation, air temperature, air pressure, albedo, incoming shortwave radiation, leaf area index, land cover and soil type. They were derived from various sources and comprised well-validated products. For precipitation forcing, the Multi-Source Weighted-Ensemble Precipitation (MSWEP) dataset was selected (<http://www.gloh2o.org/>; Beck et al., 2017). The MSWEP dataset is based on a merger of selected satellite-, reanalysis-, and gauge-based products, and is available from 1979 until 2015 at a daily  $0.25^{\circ}$  spatial resolution. The surface meteorological forcing datasets including air temperature, pressure and incoming shortwave radiation were derived from the Global Modeling and Assimilation Office (GMAO; Global Modeling and Assimilation Office, 2004) meteorological data at hourly  $1.00^{\circ} \times 1.25^{\circ}$  resolution. The GMAO datasets were also used in the calculation of MODIS NPP, GPP and ET (Running et al., 2004; Mu et al., 2007, 2011). Satellite-based inputs including leaf area index, albedo and land cover. For leaf area index and albedo, we used the 8-day  $0.05^{\circ}$  Global Land Surface Satellite (GLASS) products (<http://glassproduct.bnu.edu.cn/>; Zhao et al., 2013). This GLASS albedo was used to calculate reflected solar radiation, and hence the net incoming solar radiation (see details in Cleugh et al., 2007). Land cover were derived from yearly  $0.05^{\circ}$  MODIS products (MCD12C1) (<https://modis.ornl.gov/cgi-bin/MODIS/global/subset.pl>; Friedl et al., 2002). The land cover data was reclassified into the respective 12 PFTs of SiTH model based on International Geosphere-Biosphere Programme (IGBP) classification scheme (Belward, 1996). In addition, the required static soil texture dataset was derived from the well-regarded FAO Harmonized World Soil Database (HWSD) (<http://www.fao.org/>) at  $0.1^{\circ}$  spatial resolution. Based on the classification of United States Department of Agriculture Natural Resources Conservation Service (USDA) (USDA-NRCS, 2004), the soil texture was further divided into 11 different types defined by SiTH model. All the data sets presenting a different spatial resolution are re-

gridded to a common  $0.25^\circ \times 0.25^\circ$  spatial resolution by means of inverse distance weighted interpolation (Shepard, 1968). The daily series of leaf area and albedo were derived from the 8-day GLASS products using daily linear interpolation approach (Zhang et al., 2010). The hourly GMAO meteorological data were averaged to daily means according to the method proposed by Allen et al. (1998). To make sure that water cycle variables (i.e., soil moisture and groundwater table depth) can reach equilibrium, a 100-year spin-up was performed by repeating the forcing of the period 2000–2010 10 times. Starting from the end of the spin-up, the model was run to generate the global-scale soil moisture, groundwater table and ET products.

To compare the global ET estimated by SiTH with related ET products, five additional datasets were incorporated into the evaluation. One is the ERA-Interim reanalysis product, which is produced by the European Centre for Medium-Range Weather Forecasts (ECMWF) and covers the period from 1979 to present with a horizontal resolution of approximately  $0.7^\circ$  and 62 vertical levels (Dee et al., 2011). The other four are derived from satellite-based ET products: (1) the MOD16 ET product, which is produced based on the most widely used satellite-based ET model proposed by Mu et al. (2007, 2011). The MOD16 ET product has a spatial resolution of 1 km and is available with 8-day, monthly and annual intervals (<ftp://ftp.ntsg.umt.edu/pub/MODIS/Mirror/MOD16/>). The MOD16 ET is estimated as the sum of evaporation from water intercepted by the canopy, transpiration from the dry canopy surface, and evaporation from the moisture soil surface and saturated soil surface; (2) the GLEAM (Global Land Evaporation Amsterdam Model) product, which uses a modified PT equation in combination with an analytical rainfall interception model (Gash, 1979), a soil water module and a stress module to derive actual ET based on a wide range of remote sensing observations (Miralles et al., 2011). Data have daily  $0.25^\circ$  spatial resolution and span the 2000–2015 period (<https://www.gleam.eu/>); (3) the PT-JPL (Priestly-Taylor Jet Propulsion Laboratory) product, which applies a series of ecophysiological stress factors based on atmospheric moisture and vegetation indices into the PT equation to compute canopy transpiration, wet canopy evaporation and soil evaporation (Fisher et al., 2008). The dataset have monthly  $1^\circ$  spatial resolution and span from 1984 to 2006 (<http://landflux.org/Data.php>); (4) the PML (Penman-Monteith-Leuning) product, which uses the Penman-Monteith (PM) equation (Monteith, 1965) with a simple biophysical canopy conductance model to calculate transpiration and includes a simple term for soil evaporation, while interception loss is estimated separately using Gash rainfall interception model (Leuning et al., 2008; Zhang et al., 2008). This dataset has monthly  $0.5^\circ$  spatial resolution and span from 1981 to 2012 (<https://doi.org/10.4225/08/5719A5C48DB85>).

## 4. Results

### 4.1. Validation of *in situ* ET estimates

The statistical results for modelled versus measured daily ET at all 84 FLUXNET sites were presented in Table 3. As expected, the model performance varies from site to site. The slopes ( $b_0$ ) of the linear regression between modelled and measured daily ET ranged from 0.50 at RU-Tks to 1.35 at DK-Eng with an average of 0.83, while the intercepts ( $b_1$ ) ranged from  $-0.47 \text{ mm day}^{-1}$  at AU-DaS to  $1.09 \text{ mm day}^{-1}$  at BR-Sa1 with an average of  $0.23 \text{ mm day}^{-1}$ . The SiTh model had an average RMSE of  $0.74 \text{ mm day}^{-1}$ , ranging from  $0.29 \text{ mm day}^{-1}$  at RU-che to  $1.42 \text{ mm day}^{-1}$  at ZM-Mon. An average bias of  $0.02 \text{ mm day}^{-1}$  was obtained for all sites, ranging from  $-0.61 \text{ mm day}^{-1}$  at CZ-BK1 to  $0.68 \text{ mm day}^{-1}$  at AU-Tum. The values of NSE ranged from  $-1.07$  at ZM-Mon to  $0.80$  at CN-Ham with an average of  $0.41$ . Relatively high NSE ( $> 0.35$ ) were found at 54 sites and low NSE ( $< 0$ ) were found on at only 5 sites. On average, the model explained 65% of the variance in measured ET across all sites, ranging from a low of 23% at ZM-Mon to 88% at CA-NS6. Further details of model performances in capturing the

**Table 3**

FLUXNET2015 tower names and results of the validation of the modeled evapotranspiration (ET;  $\text{mm day}^{-1}$ ).

No.	Station	Days	$b_0$	$b_1$	$R^2$	RMSE	MBE	NSE
<b>DBF</b>								
1	CA-Oas	3680	0.67	0.30	0.68	0.68	0.02	0.68
2	CA-TPD	1010	1.17	0.66	0.71	1.00	-0.30	-0.12
3	DE-Hai	4413	1.09	-0.29	0.74	0.59	0.16	0.52
4	DE-Lnf	2599	0.54	0.28	0.66	0.70	0.25	0.59
5	DK-Sor	2638	0.56	0.27	0.67	0.78	0.34	0.57
6	IT-lsp	687	0.89	0.76	0.76	0.96	-0.59	0.57
7	IT-PT1	862	0.74	0.39	0.71	0.74	0.02	0.70
8	IT-Ro1	2055	1.05	0.24	0.69	0.61	-0.29	0.35
9	IT-Ro2	2680	0.67	0.64	0.50	0.98	-0.45	0.24
10	JP-MBF	824	0.71	0.70	0.50	0.95	-0.29	0.35
11	US-Ha1	2165	0.77	0.43	0.55	0.86	-0.14	0.44
12	US-MMs	1087	0.76	0.82	0.65	1.09	-0.12	0.39
13	US-UMD	1200	0.69	0.39	0.75	0.83	-0.19	0.56
14	US-WCr	2863	0.64	0.54	0.59	0.67	-0.04	0.74
15	US-Wi8	403	0.93	0.57	0.56	1.11	-0.45	0.18
16	ZM-Mon	669	0.79	0.39	0.23	1.42	0.09	-1.07
<b>ENF</b>								
17	CA-Man	2183	0.82	0.07	0.68	0.42	0.06	0.64
18	CA-NS5	1362	0.72	0.10	0.74	0.40	0.08	0.73
19	CA-Obs	3610	0.79	0.12	0.65	0.47	0.05	0.62
20	CA-Qfo	2597	0.99	0.30	0.60	0.62	-0.29	0.15
21	CA-SF1	1184	0.64	0.03	0.75	0.72	0.44	0.58
22	CA-TP1	4120	0.89	0.49	0.38	0.89	-0.37	-0.61
23	CN-Qia	1069	0.93	0.16	0.62	0.96	-0.03	0.47
24	CZ-BK1	2453	1.04	0.55	0.57	1.03	-0.61	0.29
25	DE-Obe	2347	0.89	0.32	0.69	0.65	-0.21	0.58
26	DE-Tha	5059	0.85	0.18	0.61	0.57	-0.00	0.52
27	FI-Let	718	0.58	0.24	0.59	0.69	0.28	0.50
28	FI-Sod	1920	0.63	0.12	0.51	0.58	0.26	0.29
29	FR-LBr	3063	0.78	0.16	0.59	0.77	0.30	0.34
30	IT-La2	415	1.20	-0.20	0.63	0.93	-0.18	0.06
31	NL-Loo	5116	0.71	0.25	0.41	0.90	0.21	-0.11
32	RU-Fyo	3956	0.81	0.13	0.68	0.79	0.22	0.41
33	US-Wi0	386	0.78	0.53	0.52	0.77	0.19	0.43
34	US-Wi5	386	0.85	0.63	0.52	0.85	-0.42	0.08
<b>EBF</b>								
35	AU-Tum	3699	0.89	-0.14	0.66	1.11	0.68	0.10
36	AU-Wac	1118	0.72	0.04	0.45	1.08	0.49	0.02
37	AU-Wom	1597	0.91	0.04	0.66	0.83	0.36	0.46
38	BR-Sa1	1367	0.92	1.09	0.54	1.10	-0.57	-0.46
39	CN-Din	1075	1.00	0.19	0.46	1.32	-0.49	-0.57
40	FR-Pue	4764	0.63	0.48	0.36	0.77	-0.12	0.08
41	IT-Cpz	2013	1.13	0.32	0.52	0.76	-0.24	-0.46
<b>MF</b>								
42	BE-Bra	4329	0.89	0.38	0.64	0.58	-0.29	0.39
43	BE-Vie	4517	0.89	0.36	0.72	0.55	-0.25	0.60
44	CA-Gro	3848	0.85	0.38	0.66	0.66	-0.23	0.54
45	US-Syv	2899	0.80	0.31	0.69	0.64	-0.08	0.66
<b>GRA</b>								
46	AT-Neu	3216	0.74	0.04	0.81	0.74	0.37	0.70
47	AU-Stp	1776	0.77	0.36	0.60	0.96	0.01	0.56
48	CH-Fru	1971	0.85	0.05	0.82	0.69	0.25	0.79
49	CH-Oe1	1876	0.82	-0.01	0.80	0.66	0.35	0.72
50	CN-Du2	918	0.81	-0.03	0.77	0.58	0.24	0.73
51	CN-Ham	943	1.02	0.02	0.84	0.44	-0.05	0.80
52	DE-Gri	3431	1.00	0.22	0.79	0.52	-0.22	0.67
53	DE-RuR	1158	0.92	-0.12	0.85	0.45	0.24	0.79
54	DK-Eng	871	1.35	-0.18	0.75	0.52	-0.18	0.17
55	IT-MBo	2809	0.75	0.27	0.78	0.62	0.14	0.77
56	NL-Hor	2808	0.75	0.18	0.71	1.12	0.39	0.28
57	RU-Ha1	522	1.02	-0.19	0.79	0.50	0.16	0.69
58	RU-Tks	443	0.50	0.10	0.57	0.62	0.38	0.31
59	US-Goo	1422	0.97	0.32	0.67	0.82	-0.27	0.47
60	US-IB2	2516	0.76	0.31	0.78	0.65	0.08	0.77
<b>SAV</b>								
61	AU-Cpr	1530	1.04	-0.05	0.54	0.55	-0.01	0.11
62	AU-DaP	1965	0.73	0.32	0.62	1.23	-0.01	0.58
63	AU-DaS	2435	1.22	-0.47	0.59	1.08	-0.12	0.11

(continued on next page)

**Table 3** (continued)

No.	Station	Days	$b_0$	$b_1$	$R^2$	RMSE	MBE	NSE
<i>Shrub</i>								
64	CA-NS6	399	1.31	0.01	0.88	0.52	-0.23	0.28
65	CA-SF3	1199	0.84	0.09	0.77	0.48	0.08	0.75
66	RU-Cok	854	0.88	-0.02	0.55	0.41	0.13	0.28
67	US-Whs	2652	0.74	0.09	0.68	0.50	0.12	0.65
68	US-SRC	1596	0.78	0.20	0.68	0.41	-0.04	0.67
<i>Wet</i>								
69	DE-Akm	610	0.77	0.23	0.74	0.54	0.09	0.73
70	DE-SFN	609	0.94	0.37	0.73	0.71	-0.29	0.59
71	DE-Spw	625	0.90	0.25	0.80	0.51	-0.14	0.77
72	DE-Zrk	527	0.70	0.31	0.78	0.64	0.10	0.76
73	DK-NuF	455	1.10	0.09	0.61	0.56	-0.17	0.14
74	FI-Lom	399	0.74	-0.01	0.69	0.75	0.48	0.30
75	RU-che	406	0.83	0.02	0.79	0.29	0.11	0.75
76	US-Ivo	590	0.64	0.14	0.67	0.46	0.10	0.64
<i>CRO</i>								
77	BE-Lon	1400	0.66	0.38	0.69	0.57	0.01	0.69
78	DE-Geb	4790	0.63	0.21	0.69	0.61	0.20	0.65
79	DE-Kli	2573	0.76	0.38	0.53	0.68	-0.12	0.42
80	FI-Jok	704	1.00	0.29	0.61	0.42	-0.09	0.32
81	FI-Gri	3326	0.60	0.04	0.64	0.80	0.54	0.32
82	IT-BCi	2685	0.61	0.37	0.43	0.94	0.49	0.12
83	US-CRT	1061	0.66	0.21	0.70	0.87	0.44	0.60
84	US-Ne2	4161	0.70	-0.02	0.78	0.99	0.59	0.65

Days: number of days with valid tower measurements;  $b_0$  and  $b_1$ : slope and intercept of the regression line between the measured and estimated evapotranspiration values;  $R^2$ : correlation coefficient; RMSE: daily root mean square error (mm/day); MAE: mean bias error (mm/day); and NSE: the Nash-Sutcliffe efficiency coefficient.

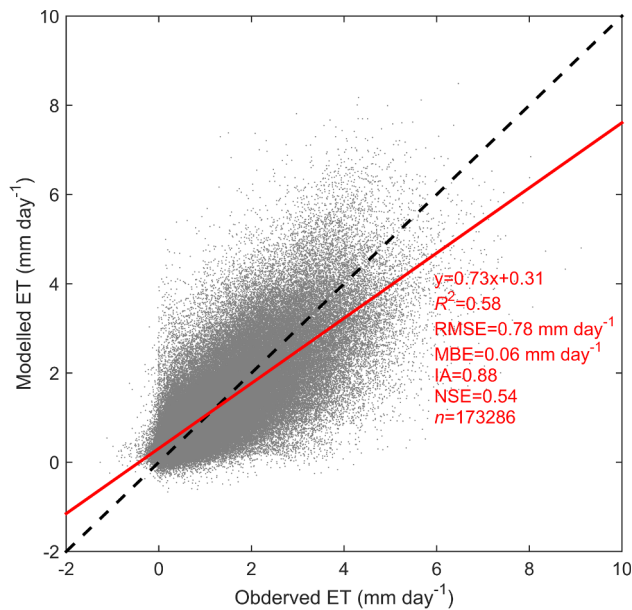


**Fig. 3.** Comparisons between daily modeled ET ( $\text{mm day}^{-1}$ ) and tower measurements for the 84 tower sites.

temporal variations of observed ET at different sites were provided in [Supplement 3](#). Overall, the model results generally agreed well with tower observations and captured observed ET seasonality and inter-annual variability over different sites. The scatterplot in [Fig. 3](#) showed modelled versus observed daily ET for all data from all 85 sites and a high correspondence of SiTH estimates with FLUXNET observations were obtained in term of relative high  $R^2$  (0.58), low RMSE ( $0.78 \text{ mm day}^{-1}$ ), low MBE ( $0.06 \text{ mm day}^{-1}$ ), high NSE (0.54) and regression slope close to one (0.73). Thus, the proposed model has the

skill to capture the daily ET over a wide range of plant types and climate conditions.

Noticeably, the model displays low values of both  $R^2$  ( $< 0.50$ ) and NSE ( $< 0$ ) at some sites of DBF (e.g., ZM-Mon), ENF (CA-TP1 and NL-Loo), EBF (BR-Sa1, and CN-Din) biomes. By examining the model performance at these sites, the causes that induced the disagreements between modelled and observed ET values were identified and illustrated by the selected sites, which were typical in representing each of the different causes. First, data errors may still exist in the latent heat flux records at some FLUXNET sites, though great efforts have been made in improving the quality of FLUXNET2015 dataset ([Pastorello et al., 2017](#)). [Fig. 4](#) represents an example of the daily time series of SiTH estimates and FLUXNET observations at site CA-TP1, which is located on the northern shore of Lake Erie in southern Ontario, Canada ([Chan et al., 2018](#)). During the period from 2002 to 2014, noisy and biased flux observations occasionally occurred and decreased the agreements between the modelled and observed ET values. Similarly, noisy and biased latent heat flux observations seemed to be occurred at other sites (i.e., NL-Loo, FR-Pue, see details [Supplement 3](#)). [Zhang et al. \(2010\)](#) also reported that an artifact of measurement errors may exist in latent heat fluxes at some FLUXNET sites. Second, soil water availability for surface evaporation and plant transpiration in SiTH model is mainly controlled by the inputs of precipitation. However, significant errors of the in situ precipitation measurements may occur at some sites due to the occasional malfunction of precipitation gages ([Dorigo et al., 2013](#)). As an example, [Fig. 5](#) illustrated that the soil moisture time series exhibited a typical wetting and consecutive drying of the soil in 2005 at ZM-Mon, while no precipitation events were recorded during the corresponding period. The errors in precipitation measurements in turn resulted in significant underestimates of ET in 2005 at ZM-Mon ([Fig. 5](#); [Table 3](#)). Third, irrigation is widely used in arid/semiarid cropland ecosystems to reduce plant drought stress by compensating for low precipitation ([Allen et al., 1998](#); [Siebert et al., 2015](#)). Because the irrigation data (the timing and amount of water applied to crops) are typically not available in the FLUXNET datasets, the soil water inputs from irrigation were not considered here. This in turn resulted in some underestimates of ET over some cropland ecosystems with irrigations during the dry periods (i.e., at site IT-BCi; [Fig. 6](#)).

#### 4.2. Validation of in situ soil moisture estimates

It should be first mentioned that most FLUXNET sites relay on time-domain reflectometry (TDR) or capacitance probes for soil moisture measurements ([Novick et al., 2016](#)), which generally need a site-specific calibration. However, details of these site-specific calibration are not generally available in the FLUXNET2015 dataset. Thus, comparisons of modelled and observed soil moisture content should be approached with caution. In addition, there is always a discrepancy between measured and modelled soil moisture in vertical scale, as the model estimates are the average of soil moisture for the surface soil layer (0–0.2 m), whereas the measurements are taken at a specific depth of the soil representing the volumetric soil water content at that level.

[Table 4](#) represents the statistical results for modelled versus observed surface soil moisture over the 38 selected FLUXNET sites. Noticeably, no local adjustment of soil hydraulic properties was made for model simulations. On average, the model explains 42% of the variance in measured surface soil water content across all sites, ranging from a low of 10% at RU-Hal to 77% at IT-Cpz. The value of RMSE varies from  $0.01 \text{ m}^3 \text{ m}^{-3}$  (at AU-Cpr) to  $0.11 \text{ m}^3 \text{ m}^{-3}$  (at DE-Tha) with a mean of  $0.05 \text{ m}^3 \text{ m}^{-3}$ . The average values of NSE (0.21) are relatively high, indicating that the patterns of temporal changes in soil moisture are well represented over a wide range of land covers and climate conditions. The details for the daily time series of surface soil moisture estimated from SiTH model versus measured data are presented in [Supplement 3](#). In most cases, the model responds properly to the

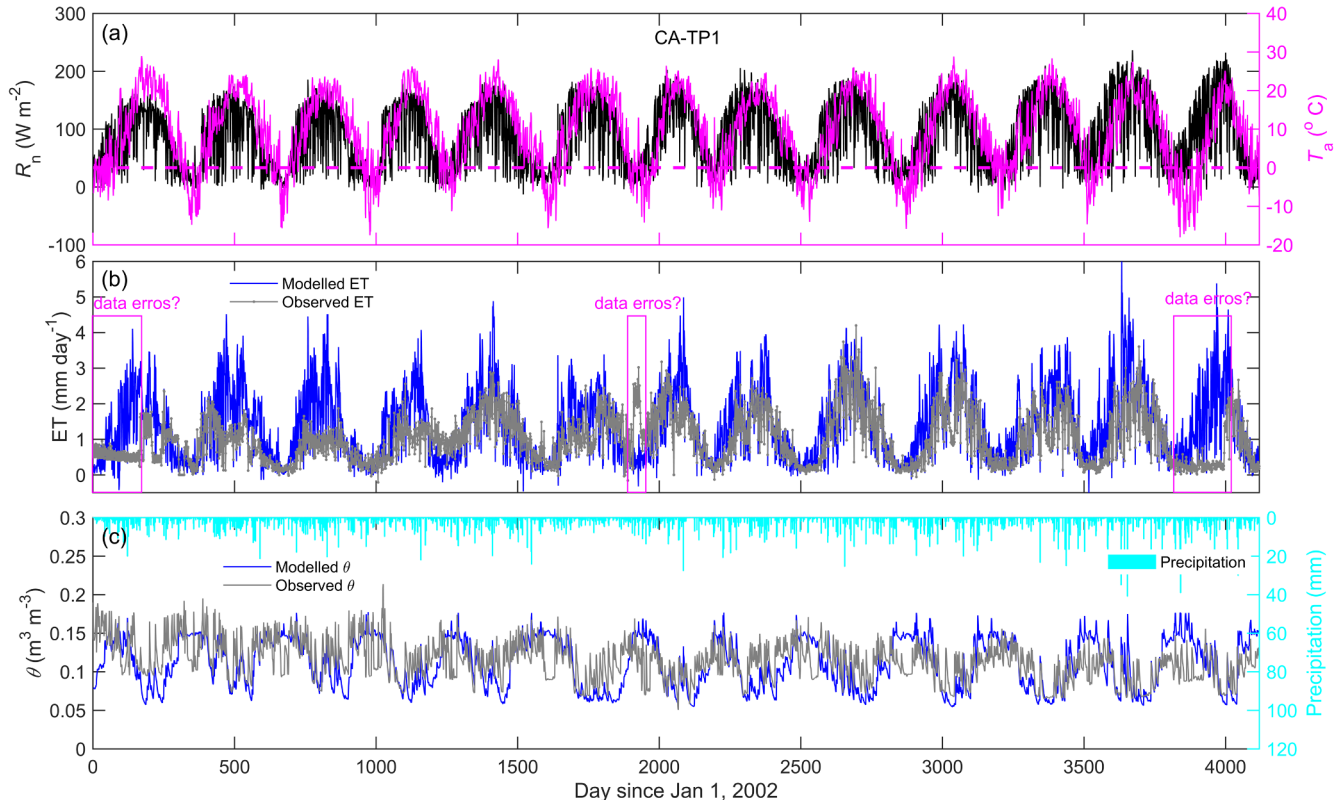


**Fig. 4.** Time series of (a) daily mean net radiation ( $R_n$ ;  $\text{W m}^{-2}$ ) and air temperature ( $T_a$ ;  $^{\circ}\text{C}$ ); (b) daily measured and modelled ET ( $\text{mm day}^{-1}$ ); and (c) precipitation (mm), modelled and measured surface soil moisture ( $\theta$ ;  $\text{m}^3 \text{m}^{-3}$ ) at site CA-TP1. The measured ET in the rectangle in subplot (b) seemed to be bias.

precipitation events and follows closely the observations during the subsequent dry-down phase, indicating the proposed soil water draining scheme (including both fast and slow draining fluxes between

layers) is reasonable.

Analogously, the causes for the differences between modelled and observed time series of surface soil moisture at some sites were

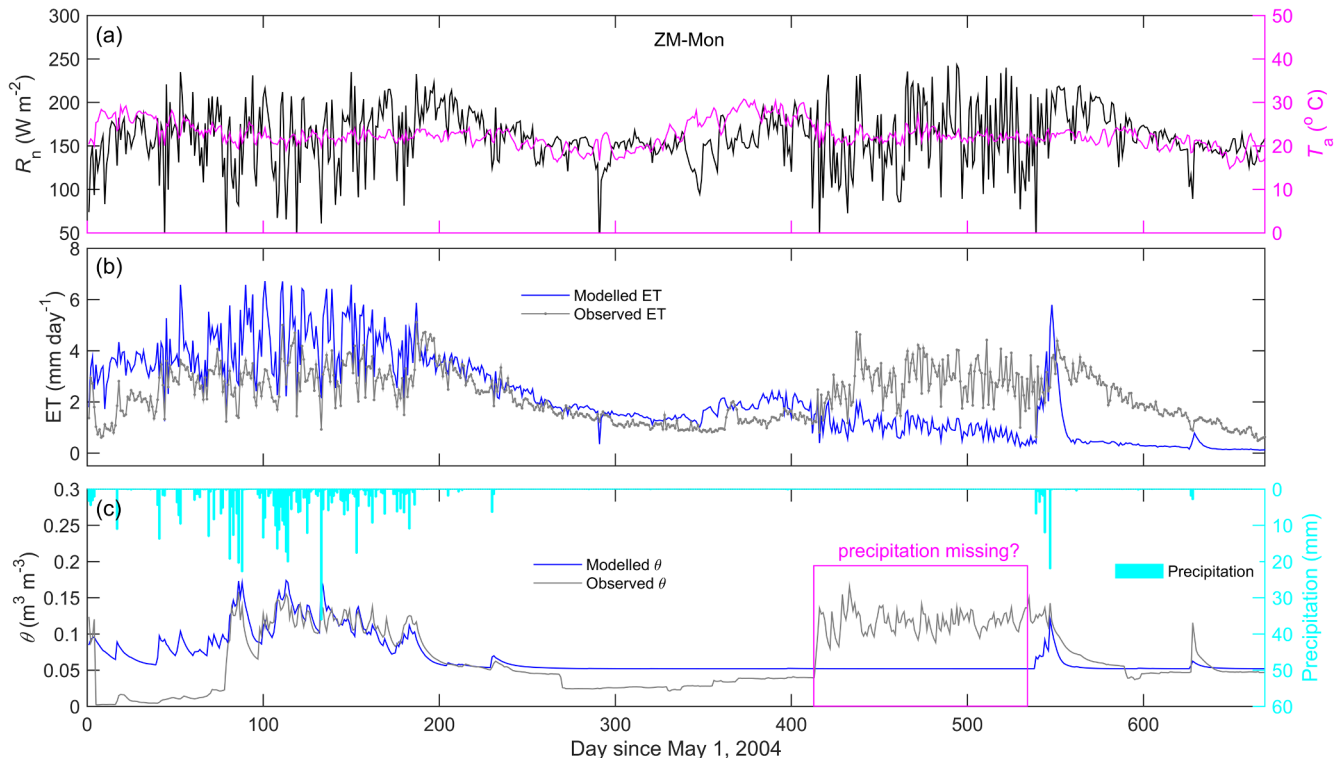


**Fig. 5.** Time series of (a) daily mean net radiation ( $R_n$ ;  $\text{W m}^{-2}$ ) and air temperature ( $T_a$ ;  $^{\circ}\text{C}$ ); (b) daily measured and modelled ET ( $\text{mm day}^{-1}$ ); and (c) precipitation (mm), modelled and measured surface soil moisture ( $\theta_1$ ;  $\text{m}^3 \text{m}^{-3}$ ) at site ZM-Mon. The precipitation in the rectangle in subplot (c) seemed to be missing.

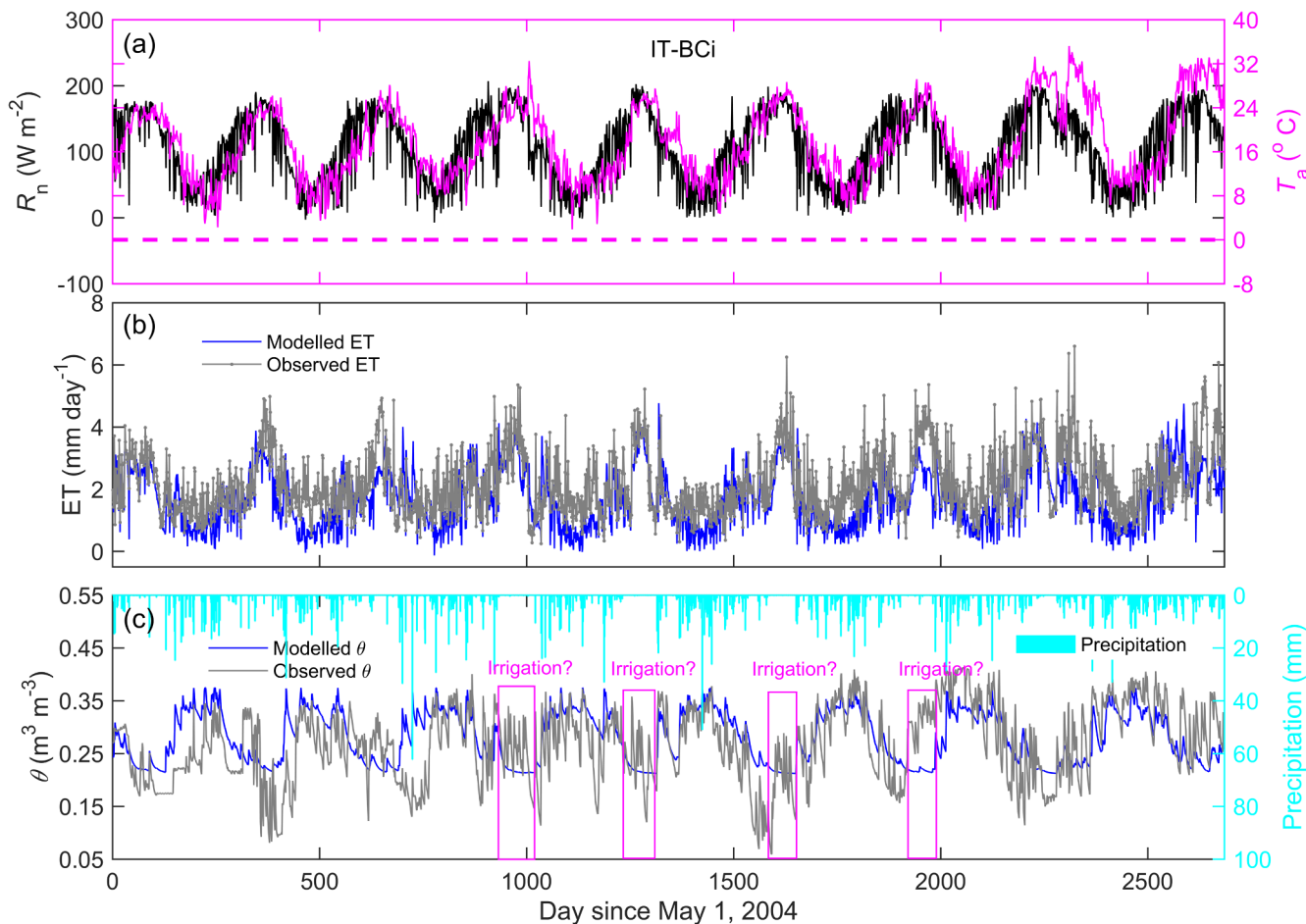


**Fig. 6.** Time series of (a) daily mean net radiation ( $R_n$ ;  $\text{W m}^{-2}$ ) and air temperature ( $T_a$ ;  $^{\circ}\text{C}$ ); (b) daily measured and modelled ET ( $\text{mm day}^{-1}$ ); and (c) precipitation (mm), modelled and measured surface soil moisture ( $\theta_1$ ;  $\text{m}^3 \text{m}^{-3}$ ) at site IT-BCi. The ET in the rectangle seemed to come from groundwater as the observed soil moisture was low.

identified as the following. First, sites with low winter temperature ( $< 0^{\circ}\text{C}$ ) have temporary conditions of the near-surface soil freeze-thaw cycles (i.e., CA-Qfo, CA-SF3, FI-Sod, US-WCr). However, our model assumes a uniform soil temperature profile throughout the soil layers that can impose inaccurate representation of the soil freeze-thaw cycles. Thus, the predicted soil moisture tended to be unrealistic during the soil freeze-thaw cycles. In addition, the accuracy of instruments to measure soil moisture in frozen soil is much lower than in unfrozen soil (Mittelbach et al., 2012). Taking both limitations into account, the difference between modelled and observed soil moisture values are expected to be high during the freezing (winter) and thawing (early spring) periods at these sites. On the contrary, the soil moisture is generally simulated with relatively high accuracy in the rest of the year (see details in Supplement 3 for sites CA-Qfo, CA-SF3, FI-Sod, US-WCr). Second, natural soil properties are highly variable and heterogeneous in both vertical and all spatial directions within a textural layer (Elkateb et al., 2003), which result in a wide variation in soil hydraulic parameters. However, we assigned homogeneous soil properties over a specific layer with a set of constant hydraulic parameters in SiTH model. The biases in hydraulic parameters may also affect the simulation results in soil moistures. Fig. 7 illustrates that the temporal pattern of surface soil moisture was adequately captured by the model at site CN-Du2. However, the model tends to overestimate soil moisture during dry season: observed soil moisture reached a minimum of  $0.046 \text{ m}^3 \text{m}^{-3}$  while the simulated minimum (wilting point) was set as  $0.139 \text{ m}^3 \text{m}^{-3}$  for loam soil (Table 2). Third, similarly to flux observations, in situ soil moisture measurements may also contain errors

due to the instrument drifts, reduced power supplies and sensor dropouts (see details in Dorigo et al., 2013). For examples, a sudden jump in the measured soil moisture were observed at site BE-Vie and it is difficult for us to establish which of the periods (i.e., before or after the jump) represents the situation closest to the truth (Fig. 8). At site DK-Sor (see details in Supplement 3), the measured soil moisture values hold constant over two long periods, which is a typical error in soil moisture observations (Mittelbach et al., 2011). Fourth, errors in soil water inputs (i.e., precipitation and irrigation) also caused the simulated soil moisture to be different from the observed values (Figs. 5 and 6 for ZM-Mon and IT-BCi, respectively).

#### 4.3. Global application

The spatial distribution and latitudinal profile of ET for 2005 modelled by SiTH was presented in Fig. 9, as well as providing five additional global ET products into evaluation. The spatial pattern was reasonable and the range of values corresponded well with other global ET products (Fig. 9). For example, the total annual ET in 2005 estimated by SiTH model was  $70.8 \times 10^3 \text{ km}^3$ , which fell with the range ( $60.6 \times 10^3$ – $83.2 \times 10^3 \text{ km}^3$ ) of the five global ET products. Among them, our estimates were very close to the results from GLEAM ( $67.4 \times 10^3 \text{ km}^3$ ) and PT-JPL ( $73.5 \times 10^3 \text{ km}^3$ ) products, but was smaller than that estimated by ERA-Interim ( $83.3 \times 10^3 \text{ km}^3$ ) and larger than that from MOD16 ( $60.6 \times 10^3 \text{ km}^3$ ) and PML ( $63.6 \times 10^3 \text{ km}^3$ ). In addition, Dirmeyer et al. (2006) reported that the mean annual global land ET ranged from  $58 \times 10^3 \text{ km}^3$  to

**Table 4**

FLUXNET2015 tower names and results of the validation of the modeled surface soil moisture.

No.	Station	Days	$b_0$	$b_1$	$R^2$	RMSE	MBE	NSE
<i>DBF</i>								
1	CA-TPD	1010	0.31	0.12	0.35	0.05	-0.01	0.20
2	DE-Hai	4413	0.80	0.07	0.44	0.07	-0.01	0.36
3	DE-Lnf	2578	0.66	0.02	0.50	0.07	-0.02	0.39
4	DK-Sor	710	0.53	0.08	0.41	0.05	0.00	0.40
5	IT-lsp	687	0.82	0.13	0.29	0.03	0.01	0.17
6	IT-Ro1	2055	1.01	-0.10	0.50	0.09	0.06	0.01
7	IT-Ro2	2680	0.54	0.06	0.35	0.10	-0.03	0.22
8	JP-MBF	822	0.44	0.27	0.20	0.09	-0.03	0.09
9	US-MMs	5087	0.47	-0.03	0.43	0.07	0.02	0.35
10	US-WCr	2863	0.53	0.22	0.13	0.07	-0.03	-0.14
11	ZM-Mon	669	0.25	0.05	0.16	0.04	0.00	0.10
<i>ENF</i>								
12	CA-Qfo	1490	0.61	0.03	0.23	0.04	0.01	-0.06
13	CA-TP1	4119	1.06	0.08	0.32	0.03	0.001	-0.29
14	CN-Qia	935	0.96	0.04	0.68	0.03	0.01	0.62
15	DE-Obe	771	0.95	-0.03	0.44	0.03	0.01	0.19
16	DE-Tha	5059	0.77	0.20	0.33	0.11	-0.08	-0.53
17	FI-Sod	1048	0.82	0.16	0.24	0.03	0.00	0.23
18	NL-Loo	724	0.97	-0.04	0.55	0.02	0.00	0.50
<i>EBF</i>								
19	AU-Wom	1597	1.30	-0.06	0.55	0.04	0.00	0.54
20	CN-Din	1075	0.94	-0.02	0.66	0.03	0.01	0.64
21	IT-Cpz	1076	0.86	-0.01	0.77	0.03	0.01	0.64
<i>MF</i>								
22	BE-Vie	1799	0.99	-0.19	0.48	0.05	0.03	-1.38
23	US-Syy	1138	0.59	0.12	0.19	0.04	0.00	-0.23
<i>GRA</i>								
24	AU-Stop	1776	0.36	0.74	0.60	0.05	-0.01	0.46
25	CH-Oei	1876	0.25	0.29	0.58	0.08	0.00	0.38
26	CN-Du2	816	0.62	-0.03	0.71	0.04	0.00	0.58
27	DK-Eng	871	0.78	0.21	0.70	0.09	0.02	0.36
28	RU-Hai	522	0.28	0.16	0.10	0.06	-0.01	0.05
29	US-Goo	1422	0.75	0.02	0.27	0.05	0.00	0.17
30	US-IB2	2518	0.61	0.06	0.34	0.07	0.02	0.25
<i>SAV</i>								
31	AU-Cpr	965	0.71	-0.03	0.45	0.01	-0.01	0.02
32	AU-DaS	2435	0.89	-0.05	0.71	0.02	0.00	0.68
33	AU-DaP	1965	0.59	-0.05	0.70	0.04	0.02	0.52
<i>Shrub</i>								
34	CA-SF3	772	0.51	0.02	0.21	0.05	0.00	0.20
<i>CRO</i>								
35	BE-Lon	2781	0.68	0.04	0.35	0.05	-0.01	0.32
36	DE-Geb	4789	0.83	0.15	0.32	0.04	0.00	0.31
37	FR-Gri	2600	0.45	0.16	0.36	0.04	0.01	0.34
38	IT-BCi	2685	0.91	-0.11	0.33	0.06	-0.01	0.31

Days: number of days with valid tower measurements;  $b_0$  and  $b_1$ : slope and intercept of the regression line between the measured and estimated surface soil moisture values;  $R^2$ : correlation coefficient; RMSE: daily root mean square error ( $\text{m}^3 \text{ m}^{-3}$ ); MAE: mean bias error ( $\text{m}^3 \text{ m}^{-3}$ ); IA: index of agreement; and NSE: the Nash-Sutcliffe efficiency coefficient.

$85 \times 10^3 \text{ km}^3$  estimated by 15 land surface models participating in the Global Soil Wetness Project 2 (GSWP-2). Jung et al. (2010) used a data-driven model tree ensemble (MTE) algorithm and derived a mean global ET of  $65 \pm 3 \times 10^3 \text{ km}^3$  over the period of 1982–2008 without considering poles and desert regions. The latitudinal profiles of annual land ET indicated that the equatorial zones had a high ET of  $1200 \text{ mm yr}^{-1}$ , while mid- and high latitude zones often had annual ET less than  $450 \text{ mm yr}^{-1}$  (Fig. 9g). Also, a major distinguishing feature of the model is the detailed estimation of ET from different water sources. Our simulations suggest that ET was mostly derived from the surface soil layer (Fig. 10a). The proportion of ET from surface soil layer varied between 40% and 90% (Fig. 10b), with a global mean of 73%. This is mainly due to the fact that at least half of root biomass is found in the upper 30 cm of soil for all vegetations globally (Schenk and Jackson,

2002a,b). The ET values from the deep soil layer were relatively high over the tropic, subtropical and boreal forests (Fig. 10c). The proportion of ET from this layer varied mostly between 10% and 30% (Fig. 10d), with a mean of 14%. Groundwater was mainly used by dry tropical savannas, temperate savannas and mediterranean shrublands (Fig. 10e and 10f), and the mean proportion of ET from groundwater was about 5% globally. The seasonal variation in ET was also well captured by SiTH model (Fig. 11). The tropical rain forest regions show year-round high ET values, while tropical dry forest and savanna regions show alternate wet [March to May (MAM) and December to February (DJF)] and dry [June to August (JJA) and September to November (SON)] seasons. The temperate and boreal-Arctic regions have much higher seasonal variability than the tropics. In the northern hemisphere, spring (MAM; Fig. 11a and b) is the onset of the growing season. ET increased and reached a peak in summer (JJA; Fig. 11c and d). In autumn (SON; Fig. 11e and f), ET began to drop and reached the minimum values in winter (DJF; Fig. 11g and h). In the southern hemisphere, it is the reverse.

Also, we examined the accuracy of SiTH model in estimating the different components of ET over different biomes and climate conditions. The spatial distribution for the different components was shown in Fig. 12, as well as providing the ratios of different components to total ET. Transpiration was the dominant component of ET and accounted for 76% of annual land ET. It was the largest in tropic and subtropical forests in South American, Africa, Asia Island, east USA and east China due to the sufficient availability of soil moisture during the plant growing seasons, but lowest in steppes of Qinghai-Tibet Plateau and major deserts of North Africa, Middle East and Middle Asia (Fig. 12a and b). For other components, soil evaporation accounted for 16% of land ET, and was important in major desert regions where most precipitation was used for  $E_s$  (Fig. 12c and d). The contribution of interception loss accounted to only 8% of land ET, and it mainly came from tropic, subtropical and boreal forests (Fig. 12e and f). The global distribution of simulated groundwater water depth was presented in Fig. 13. The spatial patterns of groundwater table depth simulated by SiTH corresponded well with previous studies (Niu et al., 2007; Fan et al., 2013; Koirala, et al., 2014). In general, the groundwater table was deeper in arid regions ( $> 10 \text{ m}$ ), whereas it was shallower in humid and high-latitude regions ( $< 5 \text{ m}$ ). In future works, a detailed study of the long-term trend of global land ET and groundwater table dynamics simulated by SiTH model will be analyzed, and we will present related results in the coming papers.

## 5. Discussion

ET remains one of the biggest unknowns within the global water balance (Miralles et al., 2011). Improved representation of its dynamics is important to facilitate our understanding of global hydrological cycles, carbon cycles and climate change. This paper presents a new model, SiTH (Simple Terrestrial Hydrosphere) that coupled parsimonious and robust models of the GSPAC, to estimate the terrestrial ET and its different components. The major distinguishing features of the methodology included that: (1) the groundwater table dynamic and its influence on soil moisture, plant transpiration and surface runoff was explicitly represented in the model based on the framework of the GSPAC, and the proportion of ET from the different water sources (e.g., surface soil layer, deep soil layer and groundwater) can also be quantified; (2) the model was built with a full modular structure and new concepts can easily be incorporated in; (3) the vertical root distributions and rooting depths of different biomes were quantified based on observation datasets (Table 1), and the effects of soil water stress on plant transpiration and soil evaporation were properly described by taking into account the influence of soil texture (Table 2); (4) the hydrological processes were represented using parsimonious and robust models. The required meteorological forcing data (i.e. air temperature, net radiation, soil heat flux and precipitation) is minimal and the static

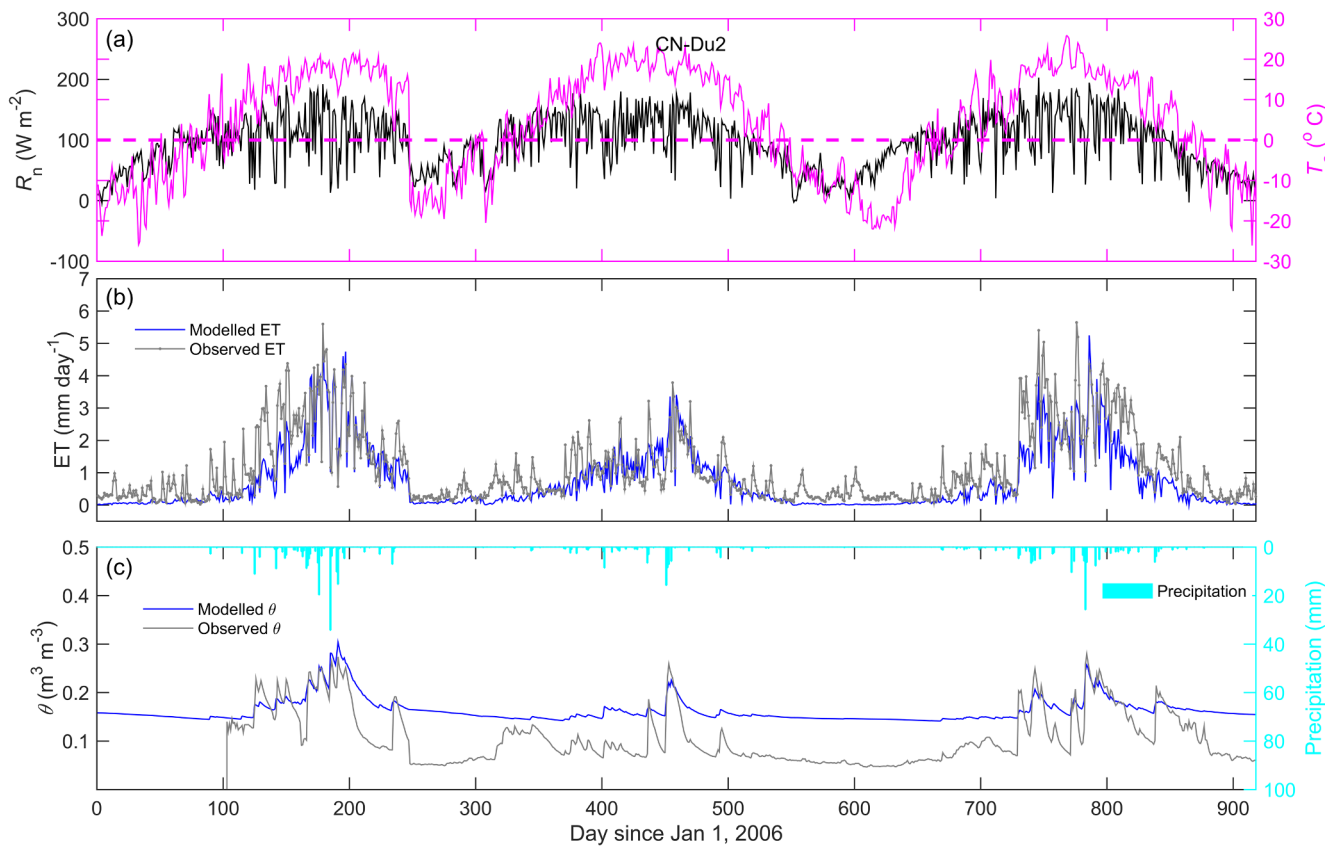


**Fig. 7.** Time series of (a) daily mean net radiation ( $R_n$ ;  $\text{W m}^{-2}$ ) and air temperature ( $T_a$ ;  $^{\circ}\text{C}$ ); (b) daily measured and modelled ET ( $\text{mm day}^{-1}$ ); and (c) precipitation (mm), modelled and measured surface soil moisture ( $\theta_1$ ;  $\text{m}^3 \text{m}^{-3}$ ) at site CN-Du2.

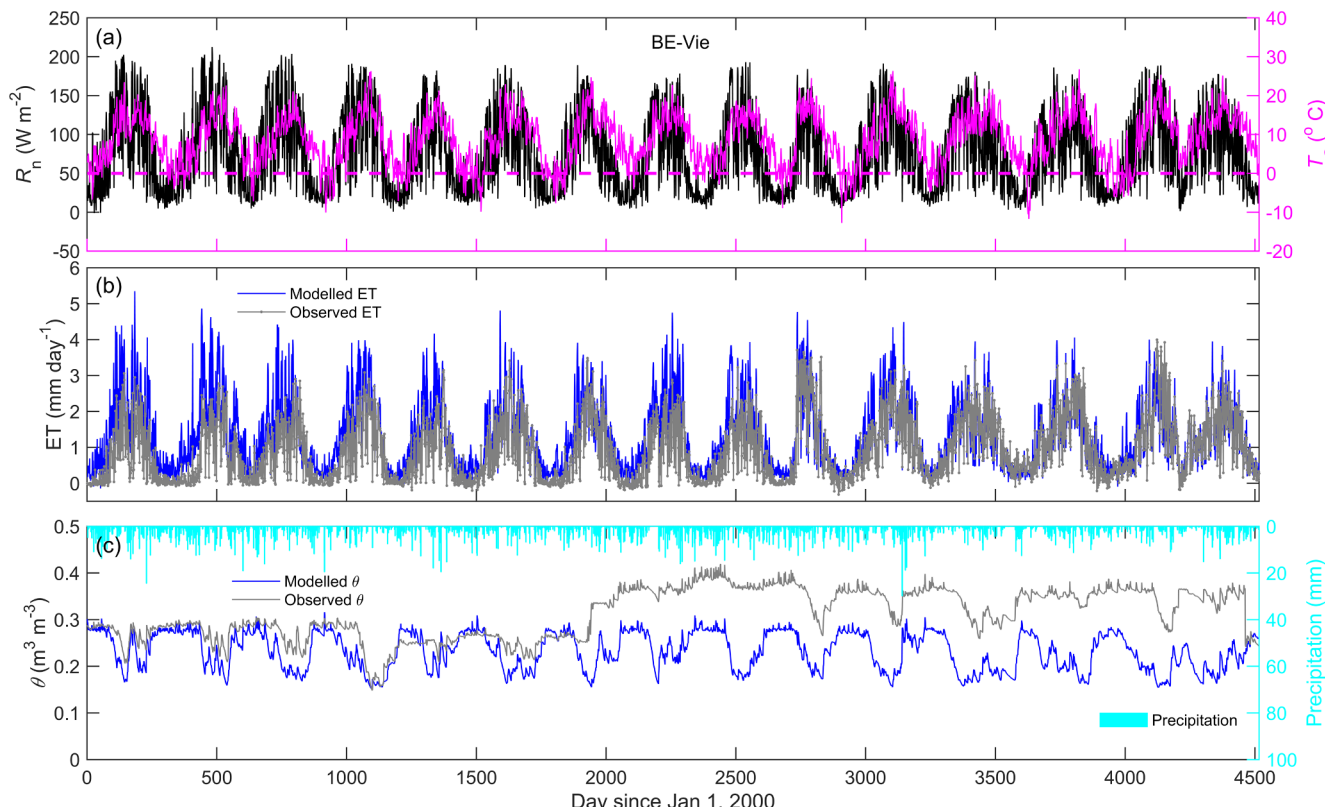


**Fig. 8.** Time series of (a) daily mean net radiation ( $R_n$ ;  $\text{W m}^{-2}$ ) and air temperature ( $T_a$ ;  $^{\circ}\text{C}$ ); (b) daily measured and modelled ET ( $\text{mm day}^{-1}$ ); and (c) precipitation (mm), modelled and measured surface soil moisture ( $\theta_1$ ;  $\text{m}^3 \text{m}^{-3}$ ) at site BE-Vie.

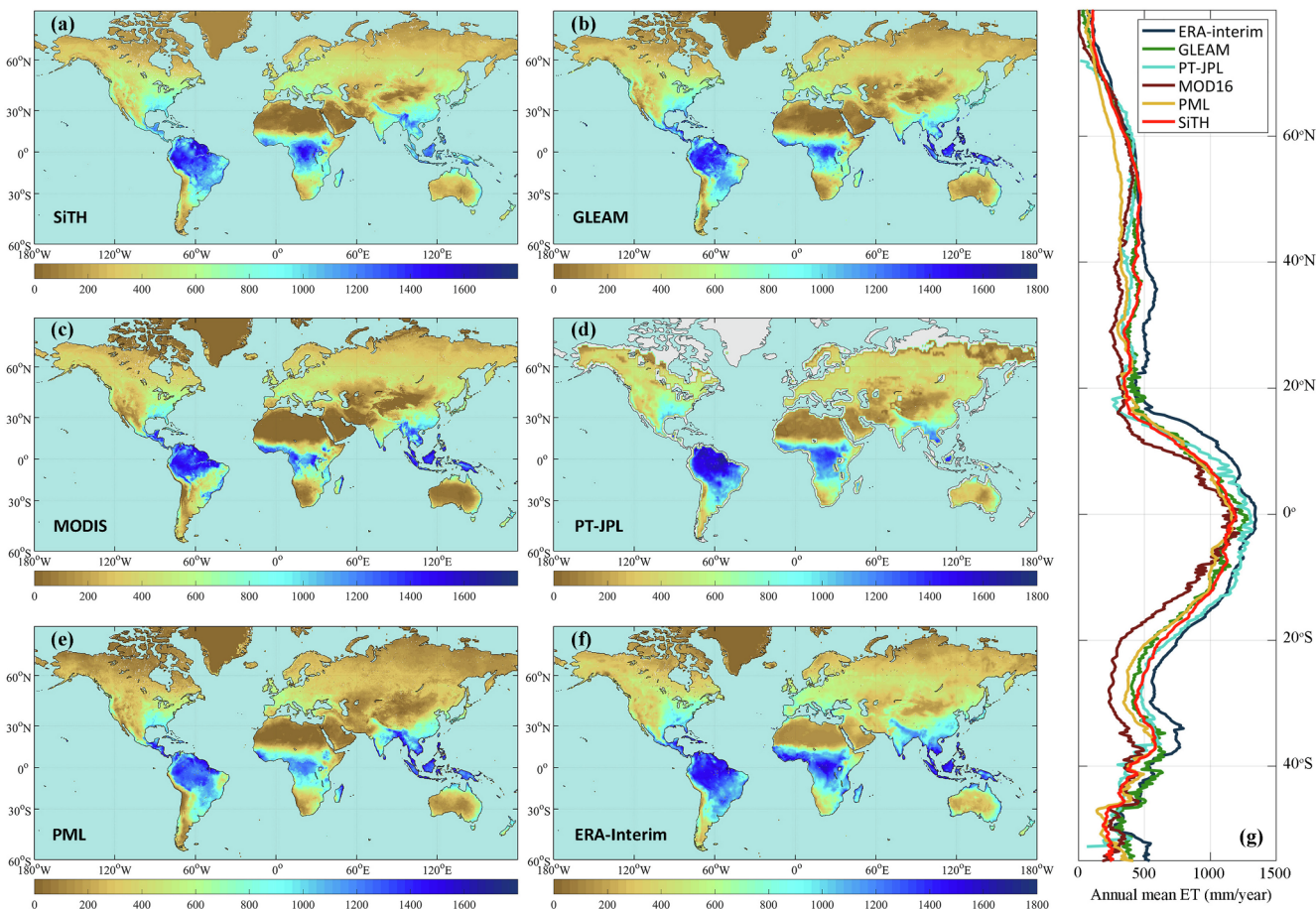


**Fig. 9.** Annual spatial patterns of ET in 2005 for (a) SiTH, (b) GLEAM, (c) MOD16, (d) PT-JPL, (e) PML, and (f) ERA-Interim; and (g) the latitudinal profiles of ET estimated by different models. The total annual ET amounts to  $70.8 \times 10^3 \text{ km}^3$  for SiTH,  $67.4 \times 10^3 \text{ km}^3$  for GLEAM,  $60.6 \times 10^3 \text{ km}^3$  for MOD16,  $73.5 \times 10^3 \text{ km}^3$  for PT-JPL,  $63.6 \times 10^3 \text{ km}^3$  for PML, and  $83.3 \times 10^3 \text{ km}^3$  for ERA-Interim.

variables (i.e. soil type and PFTs) can be easily specified from in situ measurements or existing global datasets. This simple strategy allows the application of the methodology, not only at a local scale using in situ observations, but also at a global/regional scale through the utilization of high resolution input data (i.e., satellite-retrieved LAI, land cover, etc.).

The two main intermediate products of SiTH (total ET and surface soil moisture) were compared with in situ measurements and a high correspondence of SiTH estimations with measurements was obtained over a wide variety of climate and vegetation types. It should be noticed that measurement errors in latent heat flux, soil moisture and precipitation at some sites may also degrade the statistics of validation in both ET and soil moisture estimates. Fortunately, such measurement errors only occurred occasionally, and do not significantly affect our modeling results and main conclusions drawn from daily evaluation. The estimated daily ET against eddy covariance measurements from 85 FLUXNET sites had a mean  $R^2 = 0.65$ ,  $\text{RMSE} = 0.74 \text{ mm day}^{-1}$ ,  $\text{bias} = 0.02 \text{ mm day}^{-1}$  and  $\text{NSE} = 0.41$ . The statistical results found here were comparable to that of the validations of other ET models. For example, Mu et al. (2011) reported the daily ET estimates had an average  $R^2 = 0.60$  and  $\text{RMSE} = 0.90 \text{ mm day}^{-1}$  over 46 FLUXNET sites in North America. Miralles et al. (2011) reported an average  $R^2 = 0.69$  and  $\text{RMSD} = 0.30 \text{ mm day}^{-1}$  for daily ET estimates based on a sample of 43 flux sites. Yan et al. (2012) reported that daily estimated ET had a mean  $R^2 = 0.69$ ,  $\text{RMSE} = 0.77 \text{ mm day}^{-1}$  and  $\text{bias} = -0.14 \text{ mm day}^{-1}$  over 19 flux sites. The model proposed by Fisher et al. (2010) have been extensively validated against tower measurements and has proved to estimate realistic daily and monthly ET estimates (Ershadi et al., 2014;

Michel et al., 2016; Zhu et al., 2016; Zhang et al., 2017). As an example, Zhang et al. (2017) reported an average  $R^2$  of 0.53 and NSE of  $-0.31$  for daily ET estimates against observations over 44 flux towers. The estimated surface soil moisture values were also evaluated at 35 FLUXNET sites. The results indicated that the temporal variations of the modelled and observed surface soil moisture are in good agreement with a mean  $R^2 = 0.42$ ,  $\text{RMSE} = 0.05 \text{ m}^3 \text{ m}^{-3}$ ,  $\text{bias} = -0.001 \text{ m}^3 \text{ m}^{-3}$ , and  $\text{NSE} = 0.21$  across all sites. Miralles et al. (2011) used the soil moisture data from 30 stations of the Soil Climate Analysis Network (SCAN; Schaefer et al., 2007) to validate the daily soil moisture estimates, and reported a mean  $R^2$  of 0.36 for the surface soil moisture estimates. Alavi et al. (2016) reported that daily surface soil moisture estimates of the Soil, Vegetation, and Snow (SVS) Scheme had an average  $R^2 = 0.31$  and  $\text{bias} = 0.033 \text{ m}^3 \text{ m}^{-3}$  over 130 SCAN sites. Overall, the proposed model performed relatively satisfactory in both ET and soil moisture simulations, and no systematic bias for specific biomes or climate conditions has been found. Globally, daily  $0.25^\circ$  SiTH ET simulations in 2005, which were forced using the MSWEP precipitation data, GMAO meteorological data, and GLASS land cover, leaf area index, albedo datasets, predicted an annual land ET of  $70.8 \times 10^3 \text{ km}^3$ , which fell with the range ( $60.6 \times 10^3$ – $83.2 \times 10^3 \text{ km}^3$ ) of the five global ET products, as well as the model range ( $58 \times 10^3 \text{ km}^3$  to  $85 \times 10^3 \text{ km}^3$ ) of GSWP-2 (Dirmeyer et al., 2006). The ratio of transpiration, soil evaporation and interception to total ET estimated by SiTH was 76%, 16% and 8%, respectively, which is nearly within the scope of previous studies. For example, Jasechko et al. (2013) reported that transpiration could account for nearly 80–90% of the total ET from continents by using the isotope mass balance method. This finding was criticized for overestimating the contribution of plant

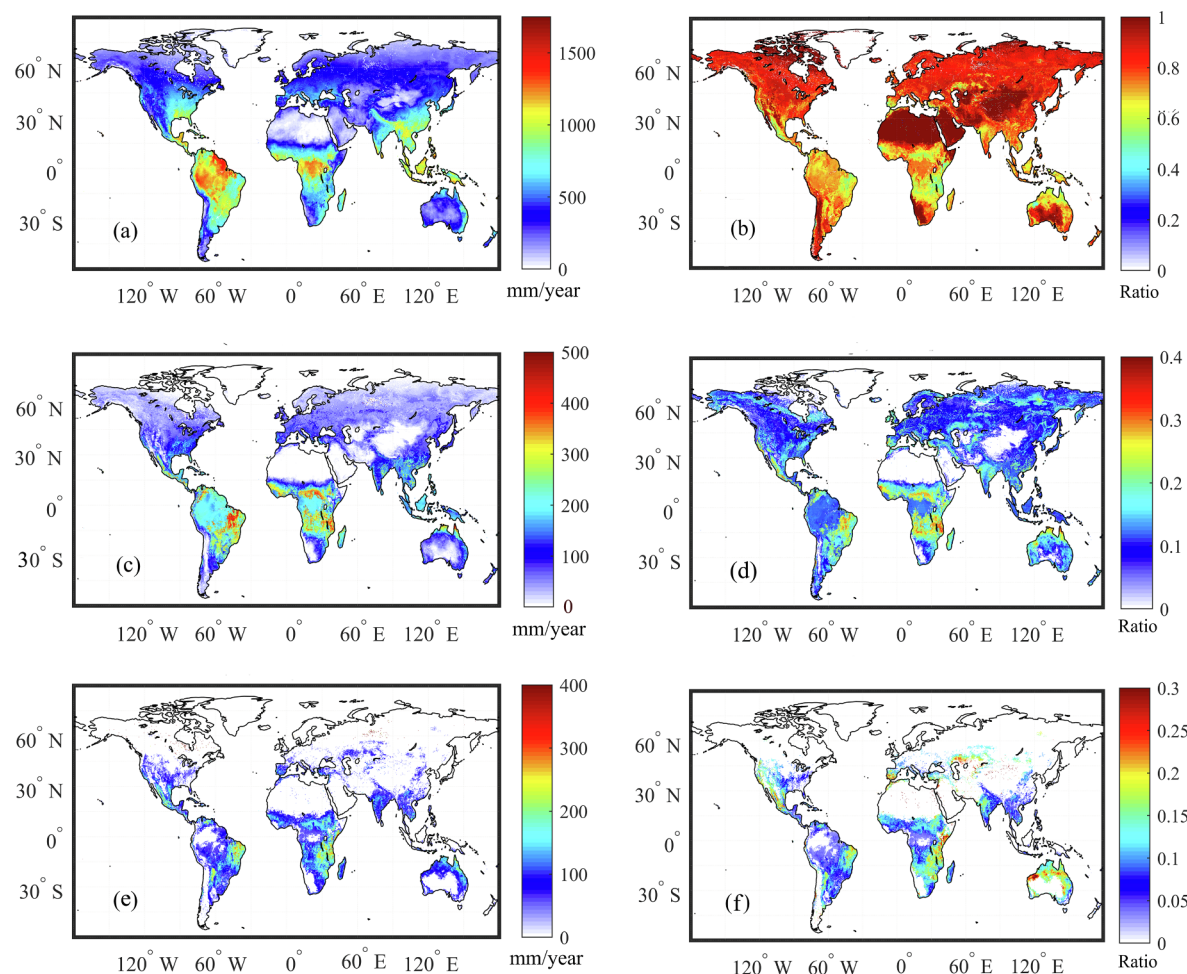


**Fig. 10.** Spatial patterns of (a) ET from the surface soil layer ( $\text{mm year}^{-1}$ ), (b) the percentage of ET from surface soil layer to total ET, (c) ET from the deep soil layer ( $\text{mm year}^{-1}$ ), (d) the percentage of ET from deep soil layer to total ET, (e) ET from groundwater ( $\text{mm year}^{-1}$ ), and (f) the percentage of ET from groundwater to total ET.

transpiration and underestimating data uncertainties. After counting the input data uncertainties, Coenders-Gerrits et al. (2014) argued the transpiration portion of ET to be lower, at 35–80%. Maxwell and Condon (2016) found transpiration accounts for  $62 \pm 12\%$  of ET by considering the influence of lateral ground water flow on ET partitioning. Previous studies reported that soil evaporation accounts for 20–40% of ET for croplands, and 5%–38% of total ET for natural vegetation (Kool et al., 2014). The ratio of global soil evaporation to total ET estimated by SiTH is comparable to that (14%) reported by Miralles et al. (2016) based on GLEAM product. Until now, direct observations on the contributions of canopy loss to total ET across different biomes are still relative sparse (Miralles et al., 2010), and estimations were mainly derived from model simulations with a range of 10–24% (Miralles et al., 2016). In addition, the spatial patterns of groundwater table depth appeared reasonable and corresponded well with previous studies (Niu et al., 2007; Fan et al., 2013; Koirala et al., 2014). Note that our current global land ET simulations were conducted using a fixed sets of forcing datasets and the errors induced by the choices of different inputs were not explored. In future studies, we will focus on analyzing the spatial and temporal variation of the global estimates of land ET and groundwater table depth over a long time period spanning from 1984 to present based on different sets of forcing inputs. Also, a detailed investigation on the proportion of ET from different water sources (e.g., surface soil layer, deep soil layer and shallow groundwater) will be conducted.

A main drawback of this study, however, was that the model assumes a uniform soil temperature profile throughout the soil layers,

which can impose inaccurate representation of the soil freeze-thaw process and adversely impact the predicted soil moisture in winter. Implementation of a soil heat diffusion scheme is currently in progress to circumvent this potential problem. In addition, the parameter values can significantly affect the simulations of soil moisture and hydrologic fluxes, and may vary with the environmental conditions, PFTs, and other factors (Zhang et al., 2017). At present, a set of constant parameters based on previous studies were used in SiTH without any calibrations. To improve model performances, there is a need to optimize the model parameters using the multiple observations (i.e., FLUXNET data, groundwater table depth, etc.) over a wide range of global bioclimatic conditions in future studies (Zhu et al., 2014; Zhang et al., 2017).

## 6. Conclusions

In this study, a relatively simple model (SiTH; Simple Terrestrial Hydrophere), that coupled the parsimonious and robust models of the GSPAC to estimate the terrestrial ET, soil moisture and groundwater table depth at the daily time scale, has been developed and evaluated. It showed good agreement with in situ observed ET and surface soil moisture at the FLUXNET sites. No systematic bias for specific vegetation types and climate conditions has been detected. As a physically-based hydrological model, SiTH has the potential for implementation at global scales. The required input data including net radiation, air temperature, precipitation, leaf area index, vegetation type and soil

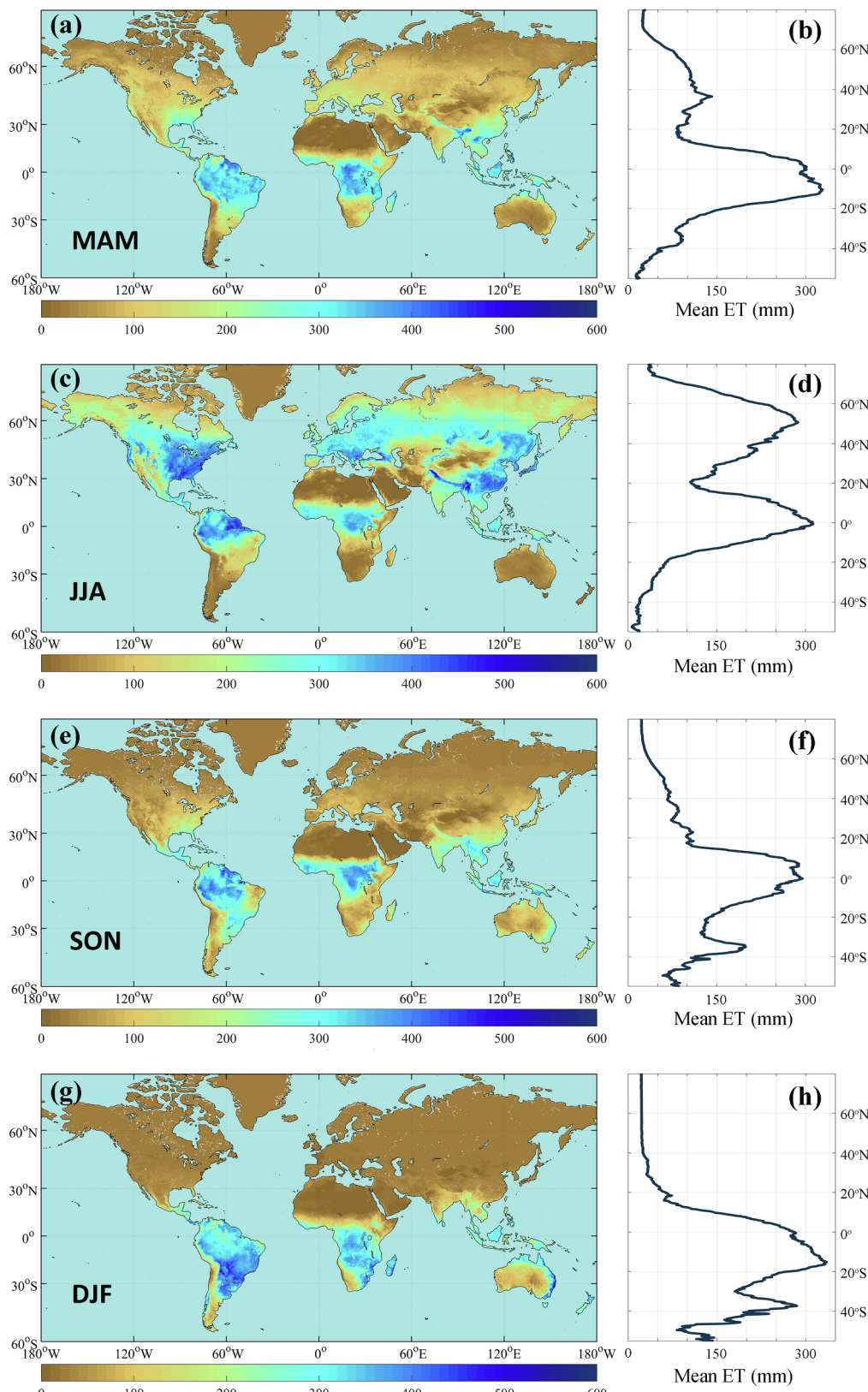


**Fig. 11.** Spatial patterns of (a) MAM, (c) JJA, (e) SON, and (g) DJF land ET based on SiTH model; and latitudinal profiles of ET in (b) MAM, (d) JJA, (f) SON, and (h) DJF.

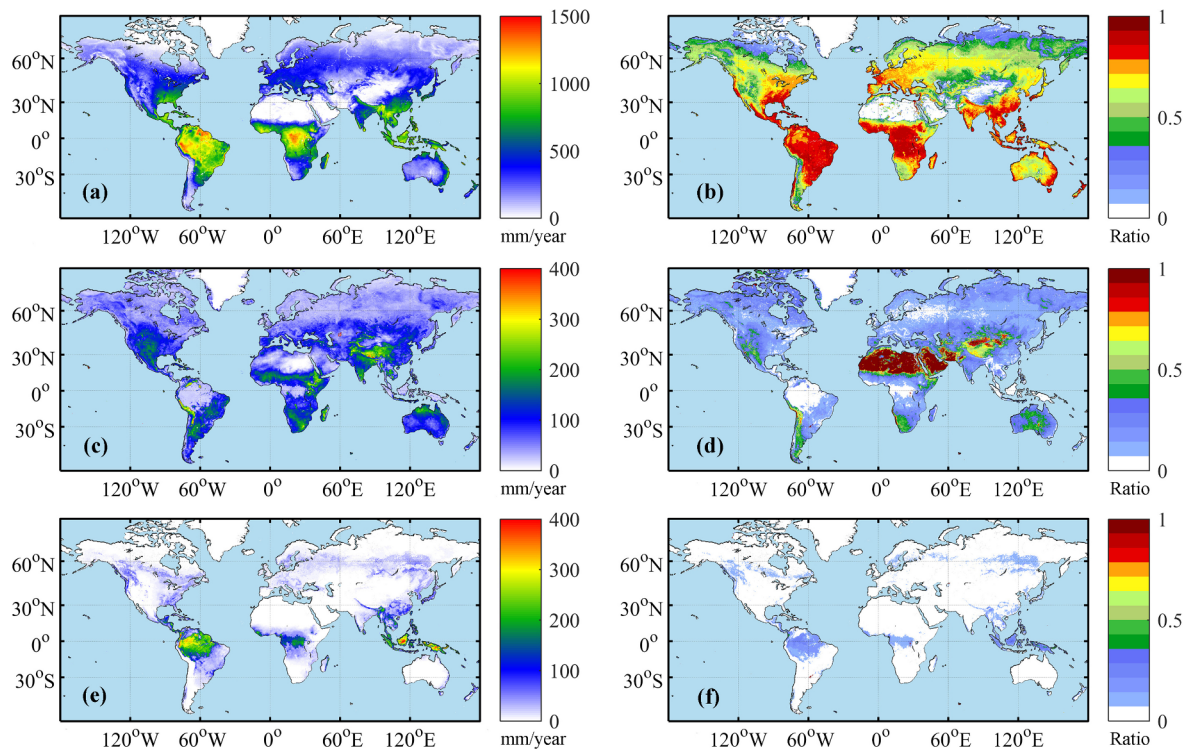


**Fig. 12.** Spatial patterns of (a) annual plant transpiration ( $\text{mm year}^{-1}$ ), (b) the percentage of plant transpiration to ET, (c) annual soil evaporation ( $\text{mm year}^{-1}$ ), (d) the percentage of soil evaporation to ET, (e) annual interception loss ( $\text{mm year}^{-1}$ ), and (f) the percentage of interception loss to ET.

data, are readily available. The estimated ET and groundwater table depth in 2005 by SiTH captured spatial and seasonal variations at the global scale and favorably compared with other estimations. In an ongoing study, we will analyze the long-term spatial and temporal variation of the global ET and groundwater table depth using different forcing input datasets. In addition, special attentions will be given to properly describe soil freeze-thaw processes in future studies.

#### Declaration of Competing Interest

We declare that we have no financial and personal relationships with other people or organizations that can inappropriately influence our work, there is no professional or other personal interest of any nature or kind in any product, service and/or company that could be construed as influencing the position presented in, or the review of, the manuscript entitled

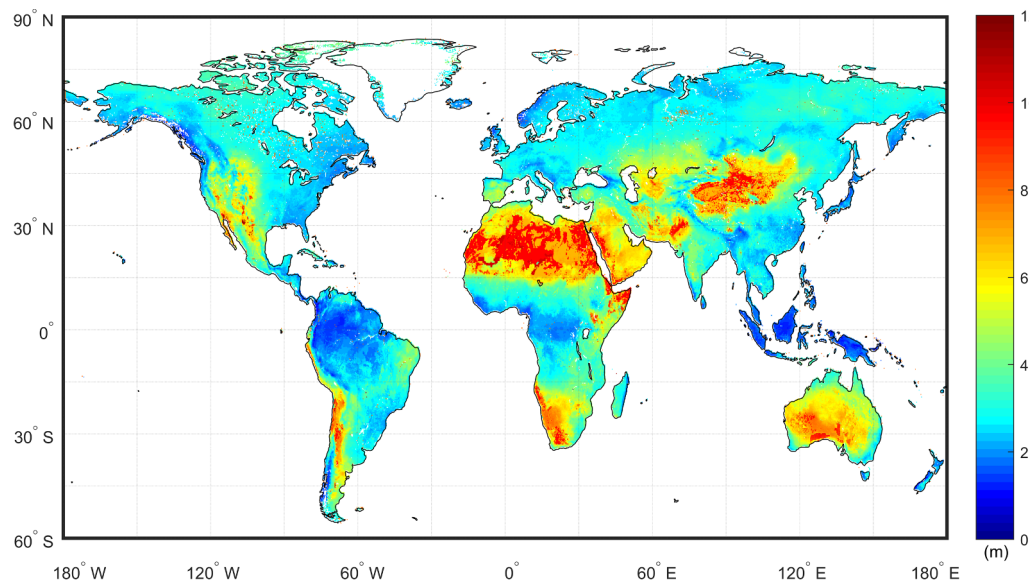


**Fig. 13.** Global distribution of simulated groundwater table depth in meters.

## Acknowledgements

This work used eddy covariance data acquired and shared by the FLUXNET community, including these networks: AmeriFlux, AfriFlux, AsiaFlux, CarboAfrica, CarboEuropeIP, CarboItaly, CarboMont, ChinaFlux, Fluxnet-Canada, GreenGrass, ICOS, KoFlux, LBA, NECC, OzFlux-TERN, TCOS-Siberia, and USCCC. The ERA-Interim reanalysis data are provided by ECMWF and processed by LSCE. The FLUXNET eddy covariance data processing and harmonization was carried out by the European Fluxes Database Cluster, AmeriFlux Management Project, and Fluxdata project of FLUXNET, with the support of CDIAC and ICOS Ecosystem Thematic Center, and the OzFlux, ChinaFlux and AsiaFlux offices. MODIS LAI satellite products were obtained online (<https://lpdaac.usgs.gov/>). This research was supported by the National Key Research and Development Program of China (2018YFC0406602), and National Natural Science Foundation of China (grants 41871078 and 41571016).

## Appendix A. Supplementary data

Supplementary data to this article can be found online at <https://doi.org/10.1016/j.jhydrol.2019.123928>.

## References

- Alavi, N., Belair, S., Fortin, V., Zhang, S., Husain, S.Z., Carrera, M.L., Abramowicz, M., 2016. Warm Season Evaluation of Soil Moisture Prediction in the Soil, Vegetation, and Snow (SVS) Scheme. *J. Hydrometeorol.* 17, 2315–2332.
- Allen, R. G., L. S. Pereira, D. Raes, Smith, M. 1998. Crop evapotranspiration- guidelines for computing crop water requirements, FAO Irrigation and Drainage Paper, No. 56, FAO, Rome.
- Beck, H.E., van Dijk, A.I.J.M., Levizzani, V., Schellekens, J., Miralles, D.G., Martens, B., Roo, A., 2017. MSWEP: 3-hourly 0.25° global gridded precipitation (1979–2015) by merging gauge, satellite, and reanalysis data. *Hydroclim. Earth Syst. Sci.* 21, 589–615.
- Belward, A.S., 1996. The IGBP-DIS Global 1 km Land Cover Data Set (DISCover): proposal and implementation plans. IGBP-DIS Working Paper 13, International Geosphere-Biosphere Programme Data and Information System Office. Toulouse, France.
- Canadell, J., Jackson, R.B., Ehleringer, J.R., Mooney, H.A., Sala, O.E., Schulze, E.-D., 1996. Maximum rooting depth of vegetation types at the global scale. *Oecologia* 108, 583–595.
- Chan, F.C.C., Arain, M.A., Khomik, M., Brodeur, J.J., Peichl, M., Restrepo-Coupe, N., Thorne, R., Beamesderfer, E., McKenzie, S., Xu, B., Croft, H., Pejam, M., Trant, J., Kula, M., Skubel, R., 2018. Carbon, water and energy exchange dynamics of a young pine plantation forest during the initial fourteen years of growth. *For. Ecol. Manage.* 410, 12–26.
- Choudhury, B.J., Idso, S.B., Reginato, J.R., 1987. Analysis of an empirical model for soil heat flux under a growing wheat crop for estimating evaporation by an infrared-temperature based energy balance equation. *Agric. For. Meteorol.* 39, 283–297.
- Choudhury, B.J., DiGirolamo, N.E., Susskind, J., Darnell, W.L., Gupta, S.K., Asrar, G., 1998. A biophysical process-based estimate of global land surface evaporation using satellite and ancillary data II. Regional and global patterns of seasonal and annual variations. *J. Hydrol.* 205, 186–204.
- Choudhury, B.J., DiGirolamo, N.E., 1998. A biophysical process-based estimate of global land surface evaporation using satellite and ancillary data I. Model description and comparison with observations. *J. Hydrol.* 205, 164–185.
- Clapp, R.B., Hornberger, G.M., 1978. Empirical equations for some soil hydraulic properties. *Water Resour. Res.* 14, 601–604.
- Clark, M.P., Fan, Y., Lawrence, D.M., Adam, J.C., Bolster, D., Gochis, D.J., Hooper, R.P., Kumar, M., Leung, L.R., Mackay, D.S., Maxwell, R.M., Shen, C., Swenson, S.C., Zeng, X., 2015. Improving the representation of hydrologic processes in Earth System Models. *Water Resour. Res.* 51, 5929–5956.
- Cleugh, H.A., Leuning, R., Mu, Q., Running, S.W., 2007. Regional evaporation estimates from flux tower and MODIS satellite data. *Remote Sens. Environ.* 106 (3), 285–304.
- Cosby, B.J., Hornberger, G.M., Clapp, R.B., Ginn, T.R., 1984. A statistical exploration of the relationships of soil moisture characteristics to the physical properties of soils. *Water Resour. Res.* 20, 682–690.
- Dee, D.P., Uppala, S.M., Simmons, A.J., Berrisford, P., Poli, P., Kobayashi, S., Andrae, U., Balmaseda, M.A., Balsamo, G., Bauer, P., Bechtold, P., Beljaars, A.C.M., van de Berg, L., Bidlot, J., Bormann, N., Delsol, C., Dragani, R., Fuentes, M., Geer, A.J., Haimberger, L., Healy, S.B., Hersbach, H., Holm, E.V., Isaksen, L., Källberg, P., Köhler, M., Matricardi, M., McNally, A.P., Monge-Sanz, B.M., Morcrette, J.J., Park, B.K., Peubey, C., De Rosnay, P., Tavolato, C., Thépaut, J.N., Vitart, F., 2011. The ERA-Interim reanalysis: configuration and performance of the data assimilation system. *Q. J. Roy. Meteorol. Soc.* 137, 553–597.
- Dirmeyer, P.A., Gao, X., Zhao, M., Guo, Z., Oki, T., Hanasaki, N., 2006. GSWP-2: multi-model analysis and implications for our perception of the land surface. *Bull. Am. Meteorol. Soc.* 87, 1381–1397.
- Dorigo, W.A., Xaver, A., Vreugdenhil, M., Gruber, A., Hegyiová, A., Sanchis-Dufau, A.D., Zamojski, D., Cordes, C., Wagner, W., Drusch, M., 2013. Global automated quality control of in situ soil moisture data from the International Soil Moisture Network. *Vadose Zone J.* 12 (3). <https://doi.org/10.2136/vzj2012.0097>.
- Elkateeb, T., Chalaturnyk, R., Robertson, P.K., 2003. An overview of soil heterogeneity: quantification and implications on geotechnical field problems. *Can. Geotech. J.* 40, 1–15.
- Ershadi, A., McCabe, M.F., Evans, J.P., Chaney, N.W., Wood, E.F., 2014. Multi-site evaluation of terrestrial evaporation models using FLUXNET data. *Agric. For. Meteorol.* 187, 46–61.
- Fan, Y., Li, H., Miguez-Macho, G., 2013. Global patterns of groundwater table depth. *Science* 339, 940–943.
- Fisher, J.B., Tu, K.P., Baldocchi, D.D., 2008. Global estimates of the land-atmosphere water flux based on monthly AVHRR and ISLSCP-II data, validated at 16 FLUXNET sites. *Remote Sens. Environ.* 112, 901–919.
- Fisher, J.B., Whittaker, R.J., Malhi, Y., 2011. ET come home: potential evapotranspiration in geographical ecology. *Glob. Ecol. Biogeogr.* 20, 1–18.
- Friedl, M.A., McIver, D.K., Hodges, J.C.F., Zhang, X.Y., Muchoney, D., Strahler, A.H., Cooper, A., Baccini, A., Gao, F., 2002. Global land cover mapping from MODIS: algorithms and early results. *Remote Sens. Environ.* 83 (1–2), 287–302.
- Gash, J.H., 1979. An analytical model of rainfall interception by forests. *Q. J. Roy. Meteorol. Soc.* 105, 43–45.
- Gerten, D., Schaphoff, S., Haberlandt, U., Lucht, W., Sitch, S., 2004. Terrestrial vegetation and water balance: hydrological evaluation of a dynamic global vegetation model. *J. Hydrol.* 286, 249–270.
- Giambelluca, T.W., Mudd, R.G., Liu, W., Ziegler, A.D., Kobayashi, N., Kumagai, T., Miyazawa, Y., Lim, T.K., Huang, M., Fox, J., Yin, S., Mak, S.V., Kasemsap, P., 2016. Evapotranspiration of rubber (*Hevea brasiliensis*) cultivated at two plantation sites in Southeast Asia. *Water Resour. Res.* 52, 660–679.
- Giardina, F., Konings, A.G., Kennedy, D., Alemohammad, S.H., Oliveira, R.S., Uriarte, M., Gentile, P., 2018. Tall Amazonian forests are less sensitive to precipitation variability. *Nat. Geosci.* 11, 405–409.
- Global Modeling and Assimilation Office, 2004. File specification for GEOSDAS gridded output version 5.3, report. Greenbelt, Md: NASA Goddard Space Flight Cent.
- Gray, D.M., Prowse, T.D., 1993. Snow and floating ice. In: Maidment, D.R. (Ed.), *Handbook of Hydrology*. McGraw-Hill, New York, pp. 7.1–7.58.
- Impens, I., Lemur, R., 1969. Extinction of net radiation in different crop canopies. *Theor. Appl. Climatol.* 17, 403–412.
- Jackson, R.B., Canadell, J., Ehleringer, J.R., Mooney, H.A., Sala, O.E., Schulze, E.D., 1996. A global analysis of root distributions for terrestrial biomes. *Oecologia* 108, 389–411.
- June, T., Evans, J.R., Farquhar, G.D., 2004. A simple new equation for the reversible temperature dependence of photosynthetic electron transport: a study on soybean leaf. *Funct. Plant Biol.* 31, 275–283.
- Jung, M., Reichstein, M., Ciais, P., Seneviratne, S.I., Sheffield, J., Goulden, M.L., Bonan, G., Cescatti, A., Chen, J., de Jeu, R., Dolman, A.J., Eugster, W., Gerten, D., Gianelle, D., Gobron, N., Heinke, J., Kimball, J., Law, B.E., Montagnani, L., Mu, Q., Mueller, B., Oleson, K., Papale, D., Richardson, A.D., Roupsard, O., Running, S., Tomelleri, E., Viovy, N., Weber, U., Williams, C., Wood, E., Zaelhe, S., Zhang, K., 2010. Recent decline in the global land evapotranspiration trend due to limited moisture supply. *Nature* 467, 951–954.
- Katul, G.G., Oren, R., Manzoni, S., Higgins, C., Parlange, M.B., 2012. Evapotranspiration: a process driving mass transport and energy exchange in the soil-plant-atmosphere-climate system. *Rev. Geophys.* 50. <https://doi.org/10.1029/2011RG000366>. RG3002.
- Kergoat, L., 1998. A model for hydrological equilibrium of leaf area index on a global scale. *J. Hydrol.* 212 (213), 268–286.
- Koirala, S., Pat, J.-F., Yeh, Y., Hirabayashi, S., Kanae, Oki, T., 2014. Global-scale land surface hydrologic modelling with the representation of water table dynamic. *J. Geophys. Res. Atmos.* 119, 75–89.
- Kool, D., Agam, N., Lazarovitch, N., Heitman, J.L., Sauer, T.J., Ben-Gal, A., 2014. A review of approaches for evapotranspiration partitioning. *Agric. For. Meteorol.* 184, 56–70.
- Laio, F., Porporato, A., Ridolfi, L., Rodriguez-Iturbe, I., 2001. Plants in water-controlled ecosystems: active role in hydrologic processes and response to water stress II. Probabilistic soil moisture dynamics. *Adv. Water Res.* 24, 707–723.
- Leuning, R., Zhang, Y.Q., Rajaud, A., Cleugh, H., Tu, K., 2008. A simple surface conductance model to estimate regional evaporation using MODIS leaf area index and the Penman-Monteith equation. *Water Resour. Res.* 44, W10419. <https://doi.org/10.1029/2007WR006562>.
- Liang, X., Xie, Z., Huang, M., 2003. A new parameterization for surface and groundwater interactions and its impact on water budgets with the variable infiltration capacity (VIC) land surface model. *J. Geophys. Res.* 108 (D16), 8613. <https://doi.org/10.1029/2002JD003090>.
- Lo, M.-H., Famiglietti, J.S., 2011. Precipitation response to land subsurface hydrologic processes in atmospheric general circulation model simulations. *J. Geophys. Res.* 116, D05107. <https://doi.org/10.1029/2010JD015134>.
- Maxwell, R.M., Condon, L.E., 2016. Connections between groundwater flow and transpiration partitioning. *Nature* 353 (6297), 377–380.
- Maxwell, R.M., Miller, N.L., 2005. Development of a coupled land surface and groundwater model. *J. Hydrometeorol.* 6, 233–247.
- Michel, D., Jiménez, C., Miralles, D.G., Jung, M., Hirschi, M., Ershadi, A., Martens, B., McCabe, M.F., Fisher, J.B., Mu, Q., Seneviratne, S.I., Wood, E.F., Fernández-Prieto, D., 2016. The WACMOS-ET project- Part 1: tower-scale evaluation of four remote-sensing-based evapotranspiration algorithms. *Hydroclim. Earth Syst. Sci.* 20, 803–822.
- Miguez-Macho, G., Fan, Y., 2012a. The role of groundwater in the Amazon water cycle: 1. Influence on seasonal streamflow, flooding and wetlands. *J. Geophys. Res.* 117, D15113. <https://doi.org/10.1029/2012JD017539>.

- Miguez-Macho, G., Fan, Y., 2012b. The role of groundwater in the Amazon water cycle: 2. Influence on seasonal soil moisture and evapotranspiration. *J. Geophys. Res.* 117, D15114. <https://doi.org/10.1029/2012JD017540>.
- Miguez-Macho, G., Li, H., Fan, Y., 2008. Simulated water table and soil moisture climatology over North America. *Bull. Am. Meteorol. Soc.* 663–672.
- Miralles, D.G., Gash, J.H., Holmes, T.R.H., De Jeu, R.A.M., Dolman, A.J., 2010. Global canopy interception from satellite observations. *J. Geophys. Res.-Atmos.* 115, D16122. <https://doi.org/10.1029/2009JD013530>.
- Miralles, D.G., Holmes, T.R.H., De Jeu, R.A.M., Gash, J.H., Meesters, A.G.C.A., Dolman, A.J., 2011. Global land-surface evaporation estimated from satellite-based observations. *Hydrol. Earth Syst. Sci.* 15, 453–469.
- Miralles, D.G., Jiménez, C., Jung, M., Michel, D., Ershadi, A., McCabe, M.F., Hirschi, M., Martens, B., Dolman, A.J., Fisher, J.B., Mu, Q., Seneviratne, S.I., Wood, E.F., Fernández-Prieto, D., 2016. The WACMOS-ET project-Part 2: evaluation of global terrestrial evaporation data sets. *Hydrol. Earth Syst. Sci.* 20, 823–842.
- Mittelbach, H., Casini, F., Lehner, I., Teuling, A.J., Seneviratne, S.I., 2011. Soil moisture monitoring for climate research: evaluation of a low-cost sensor in the framework of the Swiss soil moisture experiment (SwissSMEX) campaign. *J. Geophys. Res. D Atmos.* 116, D05111. <https://doi.org/10.1029/2010JD014907>.
- Mittelbach, H., Lehner, I., Seneviratne, S.I., 2012. Comparison of four soil moisture sensor types under field conditions in Switzerland. *J. Hydrol.* 430–431, 39–49.
- Monteith, J.L., 1965. Evaporation and the environment. *Symp. Soc. Exp. Biol.* 19, 205–234.
- Moriasi, D.N., Gitau, M.W., Pai, N., Daggupati, P., 2007. Model evaluation guidelines for systematic quantification of accuracy in watershed simulations. *Trans. ASABE* 50, 885–900.
- Mu, Q., Heinsch, F.A., Zhao, M., Running, S.W., 2007. Development of a global evapotranspiration algorithm based on MODIS and global meteorology data. *Remote Sens. Environ.* 111, 519–536.
- Mu, Q., Zhao, M., Running, S.W., 2011. Improvements to a MODIS global terrestrial evapotranspiration algorithm. *Remote Sens. Environ.* 115, 1781–1800.
- Myneni, R., Y. Knayazikhin, and T. Park (2015), MOD15A2H MODIS/Terra Leaf Area Index/FPAR 8-Day L4 Global 500m SIN Grid V006. NASA EOSDIS Land Processes DAAC. doi:10.5067/MODIS/MOD15A2H.006.
- Neptstad, D., de Carvalho, C., Davidson, E., 1994. The role of deep roots in the hydrological and carbon cycles of Amazonian forests and pastures. *Nature* 372, 666–669.
- Niu, G.-Y., Yang, Z.-L., Dickinson, R.E., Gulden, L.E., Su, H., 2007. Development of a simple groundwater model for use in climate models and evaluation with Gravity Recovery and Climate Experiment data. *J. Geophys. Res.* 112, D07103. <https://doi.org/10.1029/2006JD007522>.
- Nobuhiro, T., Shimizu, A., Kabeya, N., Tsuboyama, Y., Kubota, T., Abe, T., Araki, M., Tamai, K., Chann, S., Keth, N., 2007. Year-round observation of evapotranspiration in an evergreen broadleaf forest in Cambodia. In: Sawada, H. (Ed.), *Forest Environments in the Mekong River Basin*. Springer, Tokyo, pp. 75–86.
- Novick, K.A., Ficklin, D.L., Stoy, P.C., Williams, C.A., Bohrer, G., Oishi, A.C., Papuga, S.A., Blanken, P.D., Noormets, A., Sulman, B.N., Scott, R.L., Wang, L., Phillips, R.P., 2016. The increasing importance of atmospheric demand for ecosystem water and carbon fluxes. *Nat. Clim. Change* 6, 1023–1027.
- Oki, T., Musiakie, K., 1994. Seasonal changes of the diurnal cycle of precipitation over Japan and Malaysia. *J. Appl. Meteorol.* 33, 1445–1463.
- Pastorello, G.Z., Papale, D., Chu, H., Trotta, C., Agarwal, D.A., Canfora, E., Baldocchi, D.D., Torn, M.S., 2017. A new data set to keep a sharper eye on land-air exchanges. *Eos* 98. <https://doi.org/10.1029/2017EO007159>.
- Potter, C.S., Randerson, J.T., Field, C.B., Matson, P.A., Vitousek, P.M., Mooney, H.A., Mooney, H.A., Klooster, A.S., 1993. Terrestrial ecosystem production: a process based model based on global satellite and surface data. *Global Biogeochem. Cycles* 7, 811–841.
- Priestley, C.H.B., Taylor, R.J., 1972. On the assessment of surface heat flux and evaporation using large-scale parameters. *Mon. Weather Rev.* 100, 81–92.
- Reynolds, J.F., Kemp, P.R., Tenhunen, J.D., 2000. Effects of long-term rainfall variability on evapotranspiration and soil water distribution in the Chihuahuan desert: a modeling analysis. *Plant Ecol.* 150, 145–159.
- Richards, L.A., 1931. Capillary conduction of liquids through porous mediums. *Physics* 1, 318–333.
- Running, S.W., Nemani, R.R., Heinsch, F.A., Zhao, M., Reeves, M.C., Hashimoto, H., 2004. A continuous satellite-derived measure of global terrestrial primary production. *Bioscience* 54, 547–560.
- Scanlon, T.M., Kustas, W.P., 2012. Partitioning evapotranspiration using an eddy covariance-based technique: improved assessment of soil moisture and land-atmosphere exchange dynamics. *Vadose Zone J.* 11. <https://doi.org/10.2136/vzj2012.0025>.
- Schaefer, G.L., Cosh, M.H., Jackson, T.J., 2007. The USDA natural resource conservation service soil analysis network (SCAN). *J. Atmos. Ocean. Tech.* 24, 2073–2077.
- Schenk, H.J., Jackson, R.B., 2002b. Rooting depths, lateral root spreads and below-ground/aboveground allometries of plants in water-limited ecosystems. *J. Ecol.* 90, 480–494.
- Schenk, H.J., Jackson, R.B., 2002a. The global biogeography of roots. *Ecol. Monogr.* 72, 311–328.
- SCS, 1985. National Engineering Handbook. Section 4: Hydrology. Soil Conservation Service, U.S. Department of Agriculture, Washington, DC.
- SCS, 1986. Urban Hydrology for Small Watersheds, Technical Release No. 55. Soil Conservation Service, U.S. Department of Agriculture, Washington, DC.
- Seneviratne, S.I., Lüthi, D., Litschi, M., Schär, C., 2006. Land-atmosphere coupling and climate change in Europe. *Nature* 443, 205–209.
- Shepard, D., 1968. A two-dimensional interpolation function for irregularly-spaced data. In: *Proceedings of the 1968 23rd ACM National Conference*, pp. 517–524.
- Shugart, H.H., 2000. Ecosystem modeling. In: Sala, O.E., Jackson, R.B., Mooney, H.A., Howarth, R.W. (Eds.), *Methods in Ecosystem Science*. Springer, New York, pp. 373–388.
- Siebert, S., Kummu, M., Porkka, M., Döll, P., Ramankutty, N., Scanlon, B.R., 2015. A global data set of the extent of irrigated land from 1900 to 2005. *Hydrol. Earth Syst. Sci.* 19, 1521–1545.
- Tiktak, A., Bouting, W., 1992. Modelling soil water dynamics in a forested ecosystem. III: model description and evaluation of discretization. *Hydrol. Process.* 6, 455–465.
- Trenberth, K.E., Smith, L., 2009. The three dimensional structure of the atmospheric energy budget: methodology and evaluation. *Clim. Dynam.* 32 (7–8), 1065–1079.
- Trenberth, K.E., Smith, L., Qian, T., Dai, A., Fasullo, J., 2007. Estimates of the global water budget and its annual cycle using observational and model data. *J. Hydrometeorol.* 8, 758–769.
- Twine, T.E., Kustas, W.P., Norman, J.M., Cook, D.R., Houser, P.R., Meyers, T.P., Prueger, J.H., Starks, P.J., Wesely, M.L., 2000. Correcting eddy-covariance flux under-estimates over a grassland. *Agric. For. Meteorol.* 103 (3), 279–300.
- USDA-NRCS, 2004. Soil Survey Laboratory Manual Soil Survey Investigations Report 42 (ver. 4.0). [ftp://ftp.csc.egov.usda.gov/NSSC/Lab\\_Methods\\_Manual\\_SSIR42\\_2004\\_view.pdf](ftp://ftp.csc.egov.usda.gov/NSSC/Lab_Methods_Manual_SSIR42_2004_view.pdf).
- Wang, K.C., Dickinson, R.E., 2012. A review of global terrestrial evapotranspiration: observation, modeling, climatology, and climatic variability. *Rev Geophys.* 50, RG2005. <https://doi.org/10.1029/2011RG000373>.
- Xu, C.Y., Singh, V.P., 1998. A review on monthly water balance models for water resources investigations. *Water Resour. Manage.* 12, 31–50.
- Yan, H., Wang, S.Q., Billesbach, D., Oechel, W., Zhang, J.H., Meyers, T., Martin, T.A., Matamala, R., Baldocchi, D., Bohrer, G., Dragoni, D., Scott, R., 2012. Global estimation of evapotranspiration using a leaf area index-based surface energy and water balance model. *Remote Sens. Environ.* 124, 581–595.
- Yeh, P.J.-F., Eltahir, E.A.B., 2005a. Representation of Water Table Dynamics in a Land Surface Scheme. Part I: Model Development. *J. Climate* 18 (12), 1861–1880. <https://doi.org/10.1175/JCLI3330.1>.
- Yeh, P.J.-F., Eltahir, E.A.B., 2005b. Representation of Water Table Dynamics in a Land Surface Scheme. Part II: Subgrid Variability. *J. Climate* 18 (12), 1881–1901. <https://doi.org/10.1175/JCLI3331.1>.
- York, J.P., Person, M., Gutowski, W.J., 2002. Putting aquifers into atmospheric simulation models: an example from the Mill Creek Watershed, northeastern Kansas. *Adv. Water Resour.* 25 (2), 221–238.
- Zhang, Y.Q., Chiew, F.H.S., Zhang, L., Leuning, R., Cleugh, H.A., 2008. Estimating catchment evaporation and runoff using MODIS leaf area index and the Penman Monteith equation. *Water Resour. Res.* 44, W10420. <https://doi.org/10.1029/2007WR006563>.
- Zhang, K., Kimball, J.S., Nemani, R.R., Running, S.W., 2010. A continuous satellite-derived global record of land surface evapotranspiration from 1983 to 2006. *Water Resour. Res.* 46, W09522. <https://doi.org/10.1029/2009WR008800>.
- Zhang, K., Ma, J.Z., Zhu, G.F., Ma, T., Han, T., Feng, L.L., 2017. Parameter sensitivity analysis and optimization for a satellite-based evapotranspiration model across multiple sites using Moderate Resolution Imaging Spectroradiometer and flux data. *J. Geophys. Res. Atmos.* 122, 230–245.
- Zhao, X., Liang, S.L., Liu, S.H., Yuan, W.P., Xiao, Z.Q., Liu, Q., Cheng, J., Zhang, X.T., Tang, H.R., Zhang, X., Liu, Q., Zhou, G.Q., Xu, S., Kai, Y., 2013. The global land surface satellite (GLASS) remote sensing data processing system and products. *Remote Sens.* 5, 2436–2450.
- Zhu, G.F., Su, Y.H., Li, X., Zhang, K., Li, C., 2013. Estimating actual evapotranspiration from an alpine grassland on Qinghai-Tibetan plateau using a two-source model and parameter uncertainty analysis by Bayesian approach. *J. Hydrol.* 476, 42–51.
- Zhu, G.F., Li, X., Su, Y.H., Zhang, K., Bai, Y., Ma, J.Z., Li, C.B., Hu, X.L., He, J.H., 2014. Simultaneous parameterization of the two-source evapotranspiration model by Bayesian approach: application to spring maize in an arid region of northwest China. *Geosci. Model Dev.* 7, 741–775.
- Zhu, G.F., Li, X., Zhang, K., Ding, Z.Y., Han, T., Ma, J.Z., Huang, C.L., He, J.H., Ma, T., 2016. Multi-model ensemble prediction of terrestrial evapotranspiration across north China using Bayesian model averaging. *Hydrol. Process.* 30 (16), 2861–2879.